1991

Advances in sample introduction for inductively coupled plasma spectrometry

Daniel R. Wiederin
Iowa State University

Order Number 9126268

Advances in sample introduction for inductively coupled plasma spectrometry

Wiederin, Daniel R., Ph.D.

Iowa State University, 1991

U·M·I
300 N. Zeeb Rd.
Ann Arbor, MI 48106

Advances in sample introduction for inductively coupled plasma spectrometry

by

Daniel R. Wiederin

A Dissertation Submitted to the
Graduate Faculty in Partial Fulfillment of the
Requirements for the Degree of
DOCTOR OF PHILOSOPHY

Department: Chemistry
Major: Analytical Chemistry

Approved:

Signature was redacted for privacy.

In Charge of Major Work

Signature was redacted for privacy.

For the Major Department

Signature was redacted for privacy.

For the Graduate College

Iowa State University
Ames, Iowa
1991

TABLE OF CONTENTS

GENERAL INTRODUCTION

In the last two decades inductively coupled plasmas (ICPs) have become prominent sources for atomic emission and mass spectrometry (1-9). The growth of ICP spectrometry has paralleled its ability to perform trace multielement analyses on a ever-widening array of samples, including liquids, solids, and gases. Many developments have depended upon improvements in sample introduction methods. In fact, sample introduction has been identified as the "Achilles' heel" of ICP spectrometry (10, 11). It is reasonable, therefore, to expect that further improvements can be won from advances in sample introduction techniques.

For the ICP to effectively atomize, excite, and ionize analyte species, the sample must be introduced in a form that can be efficiently dissociated by the plasma. Usually this means that the sample is presented to the ICP as a fine aerosol. An argon stream carries the aerosol through a sample delivery tube and injects it into the center of the plasma. Aerosols have been produced directly from solid samples by arc (12, 13), spark (14-16) and laser ablation (17-23). However, the majority of samples determined by ICP spectrometry are liquids or liquid slurries of small solid particles. An aerosol is produced from liquid samples using any of a number of devices called nebulizers. A brief comparison of the most commonly used nebulizers is presented in Table I. More extensive reviews of

Table I. Comparison of major liquid nebulizer types.

Nebulizer	Configuration	Advantages	Limitations
concentric (pneumatic) (27-31)	Sample flows through inner of two concentric capillaries. Nebulizer gas exits from annular space between capillaries.	Simple, reliable for solutions with low solids content. Self-aspirating, sample liquid does not need to be pumped.	Poor analyte transport efficiency (0.5 -4 %). Subject to clogging by samples with high salt content.
cross-flow (pneumatic) (32-37)	Sample and nebulizer tubes form a right angle. Nebulizer gas blows across end of sample capillary, dispersing liquid sample.	More resistant to blockage than concentric nebulizer. May provide better long-term stability for high salt solutions.	Difficult to position capillaries precisely. Poor analyte transport efficiency.
Babington or V-groove (pneumatic) (38-41)	The sample flows over an orifice from which a gas jet emanates. The liquid is shattered when blown onto an impaction surface.	Blockage due to particles is eliminated because the sample does not flow through a small orifice. Useful for slurries.	Poor analyte transport efficiency.
frit disk (pneumatic) (42-44)	A glass frit is mounted in a tube. The sample liquid on the frit is dispersed by the nebulizer gas.	Produces a very fine mist. For low solution flow rates high analyte transport (~30 %) can be attained.	Very long clean-out time causing severe memory effects. Some solvents cause frothing.

Table I. (continued)

Nebulizer	Configuration	Advantages	Limitations
ultrasonic (45-49)	Sample liquid dispersed by ultrasonic waves generated from a piezoelectric transducer.	Produces a fine, uniform mist. Transport efficiency - 10 %. Detection limits are improved 10x over pneumatic nebulizers.	Nebulizer design is more complicated. Desolvation is required. Difficult to use with very low solution flow rates.
thermospray (50-56)	The sample is superheated as it flows through a capillary. Upon exiting, rapid boiling dissociates the sample into fine particles.	Low sample flow rates (100 μL min^{-1}) may be used. Detection limits 1x to 5x better than pneumatic. Transport efficiency -20 %.	Precision is poorer so detection limits are not as good as expected. Volatile analytes may be lost due to high heater temperatures (up to 400 ^{o}C). Requires a high pressure pump.

nebulizers have been published in the recent literature (10, 11, 24-26).

The ideal nebulizer would generate only small, uniform droplets less than 10 μm in diameter. However, the aerosol directly produced by most nebulizers (the primary aerosol) contains droplets with a wide range of sizes. It is necessary, therefore, to direct the primary aerosol through a spray chamber, where impaction and gravitational settling will remove the larger droplets (25, 57-61). The exit of the spray chamber is then connected to the the sample injector tube so that the finest droplets (the tertiary aerosol) will be delivered to the ICP.

In some situations a given nebulizer introduces too much solvent to the ICP. Such is the case when a more efficient nebulizer, such as an ultrasonic or thermospray nebulizer, is used for aqueous solutions or when volatile organic solvents are nebulized. Excess solvent will cool the plasma, resulting in depressed analyte signal. The cooler plasma will also give rise to polyatomic species which cause spectral interferences in both emission and mass spectrometry (19, 62-65). The usual way to remove the solvent is to first heat the aerosol above the solvent boiling point. The solvent is vaporized, leaving an aerosol particle containing nonvolatile analyte. Solvent vapors are then removed with varying degrees of success by passing the aerosol stream through either a membrane separator (66-70) or a condenser (45-50, 54). An aerosol composed of dried analyte is then transported to the plasma.

Although the limitations of the nebulizers listed in Table I are legion, the most significant shortcoming arises from the poor quality of the aerosol produced by the nebulizer. All of the nebulizers in Table I require a spray chamber to remove the largest droplets. As a result, on average, 98 % of the sample introduced to pneumatic nebulizers is wasted (10, 11, 24-26). The nebulizer design also determines the minimum sample size required. Because flow rates between 1 and 3 ml min^{-1} are used with most nebulizers, at least 1 ml or more of sample may be required to perform the analysis.

A second group of limitations is related to the use of a spray chamber. Residual signal arising from sample waste in the spray chamber causes a "memory effect". Memory effects occur because the spray chamber and aerosol transfer lines add volume to the system and because analyte waste from a previous sample may contribute to analyte signal during subsequent analyses. This effect is especially troublesome for relatively volatile elements such as Hg and I. Furthermore, there is evidence that noise generated in the spray chamber and sample delivery system is a source of imprecision (71).

Solvent loading effects comprise another set of sample introduction problems. As discussed above, desolvation has been used to remove part of the solvent load, however, for volatile organic solvents desolvation is often incomplete. Excessive solvent loads may compromise the detection limits or even extinguish the ICP.

The purpose of this dissertation is to describe improved sample introduction techniques for ICP spectrometry. The areas of

investigation involve the determination of metals in volatile organic solvents, the use of an improved direct injection nebulizer (DIN) for ICP mass spectrometry, measurements of the aerosol particle size distribution produced by the DIN, and application of the DIN to on-line standard additions analysis. This dissertation is presented in the alternate format. Each section stands independent of the others as a complete scientific manuscript including figures, tables, and literature cited. Additional citations from the general introduction and the summary are given after the summary.

The first section describes a multi-step cryogenic method for desolvating the aerosol produced by an ultrasonic nebulizer when volatile organic solvents such as methanol and acetonitrile are nebulized. These solvents have been characterized in the literature as being "very difficult or impossible" to analyze by ICP spectrometry (72, 73). With cryogenic desolvation, the solvent is removed to an extent that samples containing volatile organic solvents are no more difficult to analyze than aqueous samples.

A nebulizer which sprays aerosol directly into the base of the plasma for ICP mass spectrometry is investigated in the second section. This nebulizer is a modification of the direct injection nebulizer (DIN) used previously for ICP emission spectrometry (74-76). A pulseless gas displacement pump for use with the DIN is also described. The DIN does not require a spray chamber, thus, it provides 100 % analyte transport efficiency as well as substantial improvements in absolute powers of detection and precision. Use of

the DIN also reduced memory effects and is particularly convenient when sample volume is limited.

The third section describes aerosol particle size measurements from the DIN. These data provide quantitative evidence that the DIN produces an aerosol with a narrower particle size distribution than other concentric nebulizer designs.

The final section describes a method for performing on-line standard additions analyses for ICP mass spectrometry by using the DIN. The power of the method of standard additions for matrix effect correction can be applied to smaller samples at greater speeds than was previously possible.

SECTION I.

INTRODUCTION OF ORGANIC SOLVENTS INTO INDUCTIVELY COUPLED PLASMAS BY ULTRASONIC NEBULIZATION WITH CRYOGENIC DESOLVATION

Introduction

The deleterious effects of volatile organic solvents on ICPs have been reported by a number of authors (1-8). In general, plasma instability (1,6), plasma cooling (9), and spectral interferences due to molecular band emission (10) are observed when organic solvents, including those commonly used as organic modifiers for liquid chromatography, are introduced using a pneumatic nebulizer. These effects are even more severe when a highly efficient ultrasonic nebulizer is employed. A practical desolvation system which would allow ultrasonic nebulization of organic solutions would be an important advance, primarily because better detection limits are generally obtained with ultrasonic nebulizers than with pneumatic types. Possible applications requiring analysis of organic solvents include coupling the ICP with liquid chromatography, solvent extraction procedures for analyte preconcentration or the removal of matrix interferences, and determination of trace metal impurities in organic solvents.

A number of investigators have demonstrated that special conditions are required for operation of an ICP with volatile organic

solvents (1,6,11). These conditions depend both upon the solvent load and upon the nature of the pyrolysis products formed as the solvent molecules dissociate in the plasma (4,6,12). By minimizing the solvent load the effects of organic solvents on the plasma can be mitigated (5). One popular method for reducing the solvent load is to use a cooled spray chamber or a condenser to remove solvent vapors (1-7,13-15). With partial solvent stripping, however, the vapor from many volatile organic solvents still extinguishes the plasma or causes it to become unstable. Plasma operation when organic solvents are nebulized usually requires an increase in forward power compared to typical conditions for aqueous solutions. Higher power may degrade the ICP torch or reduce the lifetime of the power tube in the ICP generator (11). Also, carbon deposition on the inner tube of the torch can interrupt plasma operation (5,6,8,11,12) and molecular band emission is more severe (10) when organic solvents are nebulized.

Other measures to increase the tolerance of the plasma to organic solvents include a frit nebulizer (16), electrothermal vaporization (17), a grid-type nebulizer (7), and modifications of the torch design (18,19). Recently, removal of solvent with a jet separator (20), a momemtum-type separator (13), or a membrane separator (21-23) has been described. With the latter, the solvent vapor diffuses through the membrane to a vacuum pump, while the much larger aerosol particles remain inside the membrane tube and are swept into the ICP.

In the present work the solvent load was greatly reduced by first heating the aerosol and then transporting it through a primary

condenser kept at either 0 °C or -10 °C. After exiting the primary condenser the aerosol stream was allowed to warm before passing through a low temperature cryocondenser, which was cooled by dry ice (≃ -80 °C). This paper describes the performance of the cryogenic desolvation method during nebulization of the "difficult" solvents --methanol, acetone, acetonitrile, and ethanol. "Easy" solvents (24) such as xylene, methyl isobutyl ketone (MIBK), or chloroform may also be introduced using this system.

Experimental

Instrumentation and procedures

Operating conditions are listed in Table I. A photomultiplier tube was used for the background scans. All other data were collected using the photodiode array detector. A commercially available ultrasonic nebulizer was used. The nebulization/desolvation train is shown schematically in Figure 1. Except for the addition of the warming tube and the cryocondenser, the general scheme is similar to that described in previous papers (27-31). The heater temperature was measured using a thermocouple (27). (Caution: Since the heater temperature (Figure 1) may be higher than the flash point of the solvent, highly flammable vapors and aerosols produced from organic solvents must be kept within the inert gas stream present inside the nebulizer. The aerosol or vapor must not come in contact with the heating elements on the exterior of the heater. The fine aerosol

droplets produced by this nebulizer should not be inhaled.) When the background scans were collected the primary condenser was kept at 0 ^{o}C, otherwise the primary condenser was operated at -10 ^{o}C for organic solutions and 0 ^{o}C for aqueous solutions. Most of the solvent was removed in the primary condenser. For organic solutions, the aerosol exiting the primary condenser was allowed to warm to room temperature ($\simeq$ 20 ^{o}C) before passing through the cryocondenser.

The cryocondenser (Figure 2) was made from a 10 mm i.d. x 12 mm o.d. x 1.3 m length of pyrex tubing bent into a double loop with a radius of 8 cm. A pyrex drain tube (6 mm i.d. X 8 mm o.d.) was attached to the bottom of each loop. Condensed liquid was collected from each drain tube into a glass container which could be periodically emptied through a stopcock. The cryocondenser was cooled inside a polystyrene ice chest packed carefully with crushed dry ice. The condenser loops remained at dry ice temperature for about four hours until the dry ice sublimated away from the condenser tube. After this time, the carbon emission from the plasma slowly increased because solvent was removed less extensively as the loop gradually warmed.

A simple, inexpensive torch extension was placed on top of the torch while the background spectra were acquired. The extension excluded atmospheric gases and reduced the formation of CN, NO, and OH species at the plasma/atmosphere boundary. The torch extension was a 3 cm length of 20 mm o.d. quartz tubing without a viewing slot. Each extension lasted several hours, after which it was replaced due to

partial fogging. A disadvantage of the torch extension was that it attenuated emission signals at wavelengths lower than about 240 nm. The attenuation was more severe at shorter wavelengths, especially below 200 nm.

The extension could not be used with organic solvents unless the cryogenic desolvation apparatus was also used. If the cryocondenser was bypassed, the torch extension quickly became opaque with carbon deposits. When the cryocondenser was used for desolvation, the torch extension remained free of carbon for at least several hours. The torch extension was not used for detection limit measurements because molecular bands did not interfere significantly with the lines selected.

Each detection limit was measured as the analyte concentration necessary to yield a net signal equivalent to three times the standard deviation of the background. The standard deviation of the background was obtained from ten successive 10-second integrations at the wavelength of interest during nebulization of the appropriate solvent blank. The observation height and forward power were optimized to give the best detection limits in aqueous solution; the same conditions were then used to measure the detection limits in the various organic solvents.

Chemicals

Analytical reagent grade organic solvents were used throughout these experiments except for absolute ethanol. Methanol was obtained

from Mallinckrodt; acetone and acetonitrile were purchased from Fisher; absolute ethanol was from Midwest Grain Co. The water was purified using a Barnstead purification system. Metal stock solutions were prepared by dissolving analytical reagent grade nitrate salts of Pb, Fe, Zn, Cr, Cu, and Mg (Fisher Scientific Co.) at 1000 mg L^{-1} in AR grade methanol. Analyte solutions were made by dilution from the methanol stock solutions. All analyte concentrations were 1 mg L^{-1} except in the detection limit studies where the analyte concentrations were 40 μg L^{-1}.

Results and Discussion

ICP stability and appearance

A very intense, fine mist was observed in the spray chamber when the organic solvents were nebulized. Despite the high rate of aerosol production, the desolvation system employed in this study removed enough organic solvent from the aerosol stream so that special methods were not required to start or sustain the plasma (5-6,11). In fact, the plasma could be ignited with the aerosol gas on (1 L min^{-1}) while methanol was nebulized.

The plasma exhibited no visible green C_2 emission in the axial channel and only a little green emission around its base if the forward power was greater than 1.0 kW. The intensity of the continuum background did not change significantly whether water, methanol, acetonitrile, ethanol, or acetone was nebulized. These observations

further indicated that the desolvation system removed solvent extensively.

Characteristics of cryocondenser

After nebulization, the aerosol was heated, resulting in an aerosol stream laden with solvent vapor. As the aerosol stream cooled in the primary condenser (-10 °C) most of the solvent vapor liquefied on the walls of the condenser, but some solvent recondensed on the analyte particles. The resulting solvent droplets were observed visually at the exit of the primary condenser as a stream of fine particles flowing in the center of the aerosol tube. When the argon carrier gas warmed upon leaving the primary condenser, the organic solvent on the particles was revolatilized and the particles were no longer visible. These solvent vapors could then be removed in the cryocondenser.

A single condenser maintained at dry ice temperature removes little more solvent than a condenser at -10 °C. At lower temperatures the vapor pressure of the solvent decreases, so the solvent remains condensed on the aerosol particles. Since only the vapor phase solvent is removed by a condenser, much of the solvent on the aerosol particles would be carried through a single condenser and into the ICP.

The rate of solvent removal was measured by weighing the solvent collected at the bottom of the cryocondenser loops. When methanol was nebulized the cryocondenser removed 3.5 g/hour, which represents

several percent of the total solvent nebulized. Similar amounts were collected when other solvents were nebulized. About 90% of the liquid drained from the cryocondenser came from the first loop.

Spectra and detection limits

The background emission spectra for water and methanol in the region from 190 nm to 430 nm are compared in Figure 3. The spectra from ethanol and acetone were similar to that from methanol, except that the carbon atom lines were about twice as intense when acetone was nebulized compared to methanol. A tenfold increase in CN emission was observed when acetonitrile was nebulized compared to methanol.

Radiation below about 240 nm was not efficiently transmitted because of the quartz torch extension used to exclude atmospheric gases when background spectra were obtained. Thus the carbon line at 193.09 nm was not observed in the water spectrum and, compared to the carbon 247.86 nm line, was much weaker than expected in the methanol spectrum. The lines at higher wavelength had the same intensity either with or without the extension. The torch extension effectively eliminated emission from diatomic species formed at the outer boundary of the plasma. The extension facilitated comparison of emission from the analytical region of the plasma when different solvents were nebulized without interference due to molecular emission from the boundary regions.

Figure 3 shows that the background spectrum for methanol was quite similar to that for water. The same observation and operation

conditions were used, except that the cryocondenser was bypassed when water was nebulized. For either solvent, the primary condenser was kept at 0 °C. The intensities of the Ar I lines and the continuum background were not greatly different during nebulization of either methanol or water. Previously, without a cryocondenser small amounts of nebulized methanol extinguished the plasma (1,10,24). The results reported here indicate that when the solvent load is minimal, the plasma exhibits uniform performance regardless of the solvent nebulized.

Although the cryogenic desolvation system did remove most of the solvent, the increase in carbon line intensity (247.86 nm) when methanol was nebulized (Figure 3) showed that some solvent remained in the aerosol stream. Still the emission from CN was quite low. When methanol was nebulized without the torch extension, emission from CN dominated the spectrum, even though the cryocondenser was used. At wavelengths where spectral interference due to CN is expected, as is the case for some lines for rare earth elements (1,10), a torch extension may be necessary in addition to improved desolvation.

The detection limits for the organic solvents listed in Table II were all obtained using ultrasonic nebulization. These detection limits are essentially the same as those for water. A compromise heater temperature of 85 °C was used for all the organic solvents. For water, the recommended heater temperature (140 °C) was used (32). The detection limits in Table II for ultrasonic nebulization are all lower than the values commonly obtained when aqueous solutions are

nebulized pneumatically (i.e., the last row of Table II) (33). The detection limits in Table II are also better by factors of two to 27 than those reported for ultrasonic nebulization by Miyazaki et al. for various organic solvents (34). Their study did not employ any solvent removal techniques. The improvement factor depended mainly upon which solvent was chosen for comparison. It is important to note that the organic solvents nebulized ultrasonically in the work of Miyazaki et al. are "easy" (i.e., less volatile) solvents (5,6,24). For the solvents employed in this work, ultrasonic nebulization without at least partial desolvation promptly extinguished the plasma.

There have been very few reports of detection limits for the "difficult" solvents (5,6,24) with any nebulizer. The authors are not aware of any detection limits reported for these solvents with an ultrasonic nebulizer. The detection limits in Table II are better than the reported values for pneumatic nebulizers by factors of 6 to 100 (1,7,8,13,15).

Effect of heater and condenser

The plasma became unstable or was extinguished if any of the organic solvents were nebulized while the heater remained at room temperature ($\simeq$ 20 ^{o}C), even if the aerosol stream passed through the primary condenser (0 ^{o}C) before it entered the plasma. When the aerosol stream was heated a few degrees to 25 ^{o}C the plasma could be maintained for each solvent, although green C_2 band emission was still evident and, in the case of acetone, the plasma was somewhat unstable

at forward powers less than 1.2 kW. Alternatively, the plasma could be maintained with the heater at 20 °C if the primary condenser was cooled to -10 °C. Because of these restrictions, the primary condenser was maintained at -10 °C and the heater temperature was at least +25 °C so that the plasma could be maintained when the cryocondenser was not used. Because the primary condenser was necessary under any circumstances, it was only possible to compare the additional effects of the cryocondenser and the heater.

The effects of the temperature of the heater and the cryocondenser on C_2 molecular emission and argon atomic emission are demonstrated by Figure 4. Each spectrum was acquired using the diode array in the same wavelength region around the C_2 516.524 nm bandhead while methanol was nebulized. The plasma forward power was 1.0 kW. The primary condenser was maintained at -10 °C for the data in Figure 4. The spectrum shown in Figure 4a was acquired while both the heater (+80 °C) and the cryocondenser (-80 °C) were used. Figure 4d was acquired under the same conditions except that the cryocondenser was bypassed and the heater was set at only +25 °C. The C_2 molecular emission decreased by a factor of 25 and argon atomic emission increased by a factor of 5 when both the cryocondenser and heater were used in the desolvation process (Figure 4a) compared to partial desolvation at a condenser temperature of -10 °C and a heater temperature of +25 °C (Figure 4d).

The effects caused by using the cryocondenser and the heater independently are shown in Figure 4b and Figure 4c, respectively. In

each case emission from C_2 was substantially less than that observed when neither the cryocondenser nor the heater was used. However, C_2 intensity was greater than when the complete heater-cryocondenser system was used. Emission from argon was 25% less intense in Figure 4b and 37% less intense in Figure 4c than it was when the complete desolvation system was used. Figure 4c shows that "difficult" organic solvents can be introduced into the plasma using only the heater and single condenser in the present commercial ultrasonic nebulizer, although the additional cryocondenser is clearly preferable.

The weak C_2 emission observed in Figure 4a disappeared within 20 seconds after turning the nebulizer power off; this time period is comparable to the void time of the spray chamber and tubing. Liquid methanol waste was still present in the nebulizer spray chamber, but very little methanol reached the plasma. This observation suggests that the C_2 emission observed in Figure 4a is due to solvent which is carried into the plasma in the nebulized aerosol particles, and not as solvent vapor. Thus, the desolvation system might be improved to remove an even greater fraction of the solvent, possibly by using more than one cryocondenser with a warming step between each one.

The effects of heater temperature on the intensities of Zn, Fe, Mg and C lines for four organic solvents are shown in Figure 5. The cryocondenser was used in each experiment. For the analyte lines (Mg, Zn, and Fe) the maximum intensities occurred when the heater temperature was higher than 50 ^{o}C. At heater temperatures greater than about 30 degrees above the boiling point of the solvent, analyte

intensities decreased. Loss of analyte emission at excessive heater temperatures has been noted previously for aqueous samples (27,31). Carbon intensities, on the other hand, decreased as the heater temperature increased, up to the approximate boiling point of the solvent. At heater temperatures higher than the solvent boiling point the carbon intensity increased slightly. This trend is similar to a previous observation by Fassel and Bear, who noted that in the higher range of heater temperatures (> 150 ^{o}C) more water left the condenser (27).

For the organic solvents shown in Figure 5, heating the aerosol stream yielded a 2 to 3 fold increase in analyte emission intensity and a 2 fold decrease in C I intensity. The authors believe that this is due primarily to improved desolvation when the heater is used. The heater effect illustrates the need for temperature control both in experiments using this system and in other systems in which a condenser is placed in the aerosol line. The reasons for significant changes in Fe and Zn emission intensity in Figure 5 when different solvents are used are unclear at this time.

Classically, desolvation of aerosols in heated chambers has suffered from memory effects and analyte losses, especially for analytes with high vapor pressures. Such analytes may be volatilized in the heater and then removed in the condensers. Previous studies with ultrasonic nebulizers using aqueous solutions indicated that aerosol temperatures above 120 ^{o}C caused loss of volatile species containing elements such as Hg and B (27). Similar problems have also

been encountered by the authors during nebulization of Os and Re in aqueous solutions. For the solvents studied in this work desolvation is required, and some heating is desirable. Many organic solvents have lower boiling points than water, so lower heater temperatures ($\simeq$ 80 ^{o}C) are adequate. Thus, the authors do not anticipate that analyte loss or memory effects will prove any worse for organic solvents than for aqueous solutions.

The effect of forward power on emission from the C_2 bandhead as a function of both heater temperature and condenser temperature while methanol was nebulized is shown in Figure 6. The lack of some data points for powers of 0.5 kW and 0.75 kW indicates conditions where the plasma extinguished because the power was too low to overcome the heavy solvent loading. The C_2 emission signal is smallest, i.e., desolvation is most efficient, when both the heater and the cryocondenser are used. Under these conditions the C_2 band intensity changes little with increasing forward power, indicating that the solvent load has been sufficiently reduced so that the residual solvent has little effect on the plasma.

Kreuning and Maessen (4) have suggested that conditions that yield only weak C_2 spectra correspond to extensive dissociation of molecules in the plasma. If so, the lowest curve in Figure 6 suggests that when both the heater and the cryocondenser are utilized for desolvation, the dissociation processes are extensive at a forward power as low as 1.0 kW. However, when only minimal heating (25 ^{o}C) and a condenser

temperature of -10 °C are employed, dissociation is not extensive even at 1.75 kW.

Figure 7 shows that argon emission intensity is highest when the heater temperature is 80 °C and the cryocondenser is cooled to -80 °C. These conditions also produce the lowest C_2 emission (Figure 6), indicating extensive desolvation. Compare this datum curve to that obtained with a heater temperature of 25 °C and a condenser temperature of -10 °C (partial desolvation). These two curves are separated by a power increment of about 0.5 kW, as shown by the arrows in Figure 7. Others have found that, with conventional sample introduction techniques, the excitation properties of an "organic" plasma are similar to those from an "aqueous" plasma if the power is increased by 0.5 kW for the "organic" plasma (9,19). With the cryogenic desolvation system, the excitation properties (i.e., background spectra and analyte line intensities) are similar for both organic solutions and aqueous solutions at the same forward power. The need for the higher power to revitalize the plasma when using an organic solvent is eliminated by reducing the solvent load.

Conclusion

The literature reports a wide variety of conditions required for operating ICPs with organic solutions, depending strongly upon the solvent (18). We have presented a method that reduces the solvent load to such an extent that a single set of conditions works for a

range of solvents. Special torches, plasma ignition conditions, sample delivery restrictions, or higher forward powers are not required for sustenance of a stable plasma.

This desolvation system could be used when organic solvents or the effluent from a liquid chromatograph is nebulized into less robust plasmas, such as lower power microwave induced plasmas and helium ICPs. The system may also facilitate the use of low power, low flow ICP torches for liquid chromatography. In ICP mass spectrometry, cryogenic desolvation attenuates many solvent-derived polyatomic ions and alleviates the corresponding overlap interferences from either aqueous or organic solvents (35,36). An electronic cooling system capable of reaching -80 ^{o}C (rather than the solid dry ice packing) should allow continuous, indefinite operation of the cryogenic desolvation system.

Literature Cited

1. Boorn, A. W.; Browner, R. F. Anal. Chem. 1982, 54, 1402-1410.
2. Hausler, D. W.; Taylor, L. T. Anal. Chem. 1981, 53, 1223-1227.
3. Hausler, D. W.; Taylor, L. T. Anal. Chem. 1981, 53, 1227-1231.
4. Kreuning, G.; Maessen, F. J. M. J. Spectrochim. Acta, Part B 1989, 44B, 367-384.
5. Maessen, F. J. M. J.; Kreuning, G.; Balke, J. Spectrochim. Acta, Part B 1986, 41B, 3-25.
6. Maessen, F. J. M. J.; Seeverens, P. J. H.; Kreuning, G. Spectrochim. Acta, Part B 1984, 39B, 1171-1180.
7. Brotherton, T.; Barnes, B.; Vela, N.; Caruso, J. J. Anal. At. Spectrosc. 1987, 2, 389-396.
8. Barrett, P.; Pruszkowska, E. Anal. Chem. 1984, 56, 1927-1930.
9. Blades, M. W.; Caughlin, B. L. Spectrochim. Acta, Part B 1985, 40B, 579-591.
10. Xu, J.; Kawaguchi, H.; Mizuike, A. Anal. Chim. Acta 1983, 152, 133-139.
11. Seeverens, P. J .H.; Klaassen, E. J. M.; Maessen, F. J. M. J. Spectrochim. Acta, Part B 1983, 38B, 727-737.
12. Boorn, A. W.; Cresser, M. S.; Browner, R. F. Spectrochim. Acta, Part B 1980, 35B, 823-832.
13. Brotherton, T. J.; Pfannerstill, P. E.; Creed, J. T.; Heitkemper, D. T.; Caruso, J. A.; Pratsinis, S. E. J. Anal. Atomic Spectrosc. 1989, 4, 341-345.

14. Magyar, B.; Lienemann, P.; Vonmont, H. Spectrochim. Acta, Part B 1986, 41B, 27-38.

15. Ebdon, L.; Evans, E. H.; Barnett, N. W. J. Anal. At. Spectrom. 1989, 4, 505-508.

16. Nisamaneepong, W.; Haas, D. L.; Caruso, J. A. Spectrochim. Acta, Part B 1985, 40B, 3-10.

17. Ng, K. C.; Caruso, J. A. Anal. Chem. 1983, 55, 2032-2036.

18. Ng, R. C.; Kaiser, H.; Meddings, B. Spectrochim. Acta, Part B 1985, 40B, 63-72.

19. Boumans, P. W. J. M.; Lux-Steiner, M. Ch. Spectrochim. Acta, Part B 1982, 37B, 97-126.

20. Gustavsson, A. Spectrochim. Acta, Part B 1987, 42B, 111-118.

21. Backstrom, K.; Gustavsson, A.; Hietala, P. Spectrochim. Acta, Part B 1989, 44B, 1041-1048.

22. Gustavsson, A. Spectrochim. Acta, Part B 1988, 43B, 917-922.

23. Gustavsson, A. Trends Anal. Chem. 1989, 8, 336-338.

24. Miyazaki, A.; Kimura, A.; Bansho, K.; Umezake, Y. Anal. Chim. Acta 1982, 144, 213-221.

25. Winge, R. K.; Fassel, V. A.; Edelson, M. C. Spectrochim. Acta, Part B 1988, 43B, 85-91.

26. Scott, R. H.; Fassel, V. A.; Kniseley, R. N.; Nixon, D. E. Anal. Chem. 1974, 46, 75-80.

27. Fassel, V. A.; Bear, B. R. Spectrochim. Acta, Part B 1986, 41B, 1089-1113.

28. Olson, K. W.; Haas, W. J., Jr.; Fassel, V. A. Anal. Chem. 1977, 49, 632-637.

29. Goulden, P. D.; Anthony, D. H. J. Anal. Chem. 1984, 56, 2327-2329.

30. Veillon, C.; Margoshes, M. Spectrochim. Acta, Part B 1968, 23B, 553-555.

31. Boumans, P. W. J. M.; DeBoer, F. J. Spectrochim. Acta, Part B 1976, 31B, 355-375.

32. Chan, S. K.; Rohde, M. D.; Davidson, J. Technical Note No. 120189; Cetac Technologies: Omaha, NE, 1989.

33. Winge, R. K.; Peterson, V. J.; Fassel, V. A. Applied Spectrosc. 1979, 33, 206-219.

34. Miyazaki, A.; Kimura, A.; Tao, H.; Bansho, K.; Umezaki, Y. Bunseki Kagaku 1983, 32, 746-751.

35. Houk, R. S.; Smith, F. G.; Wiederin, D. R.; Niu, H. Presented at 16th Ann. Mtg. Fed. Anal. Chem. Spectrosc. Soc. (FACSS), Chicago, IL, 1989; abstract 592.

36. Houk, R. S.; Wiederin, D. R.; Smith, F. G.; Winge, R. K.; Shum, C. K. Presented at Winter Conf. Plasma Spectrochem., St. Petersburg, FL, 1990; abstract IL12.

Table I. Experimental facilities and operating conditions.

Monochromator (25)	McPherson M2051, 1 m focal length. Holographic grating: 3600 grooves/mm for $\lambda < 430$ nm, 1800 grooves/mm optimized for 450 to 850 nm used for $\lambda > 430$ nm. Entrance slit width = 20 μm
ICP generator	Plasma-Therm HFS 5000D, 27.12 MHz: variable forward power (0.5 kW to 1.75 kW) 1.25 kW for detection limit work
ICP·torch	Fassel-type (26)
Argon flow rates:	
outer	16 L min^{-1}
auxiliary	0.4 L min^{-1}
aerosol carrier	1.0 L min^{-1}
Observation position	15 mm above load coil
Nebulizer	Cetac U-5000 ultrasonic nebulizer current setting = 5.5 (arb. units) heater temperature: as indicated
Sample flow rate	3.0 ml/min
Cryocondenser temperature	$\simeq$ -80 ^{o}C
Detectors	Princeton Applied Research, Model 1453 photodiode array, unintensified, cooled to -15 ^{o}C. ENI-Gencom PMT RFI/B-289F (-800 V) used for background spectra.

Table II. Detection Limits in Organic Solvents with Cryocondenser.

Solvent	Detection limit ($\mu g\ L^{-1}$) for line indicated				
	Zn I 213.856	Pb II 220.353	Fe II 259.940	Cr II 267.716	Cu I 324.754
Methanol	0.2	4	0.2	0.4	0.2
Ethanol	0.3	5	0.6	0.8	0.3
Acetonitrile	0.4	5	0.3	0.6	0.2
Acetone	0.3	4	0.5	0.5	0.4
Water[a] (ultrasonic)	0.4	5	0.4	0.5	0.5
Water[b] (pneumatic)	1.8	42	6.2	7.1	5.4

[a] Detection limits from this work without cryocondenser.

[b] Typical detection limits with pneumatic nebulizer, Reference (25).

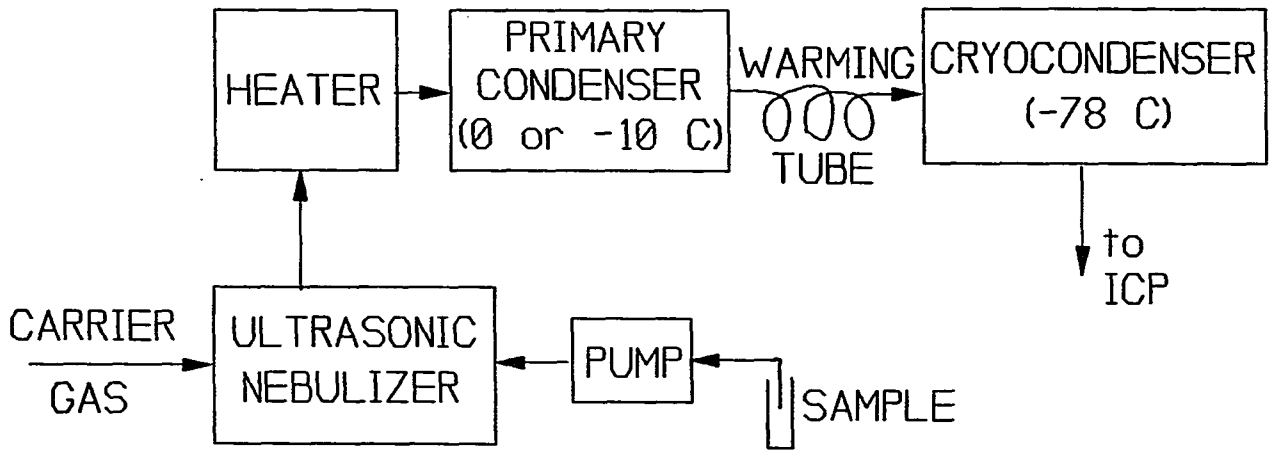

Figure 1. Diagram of the desolvation system.

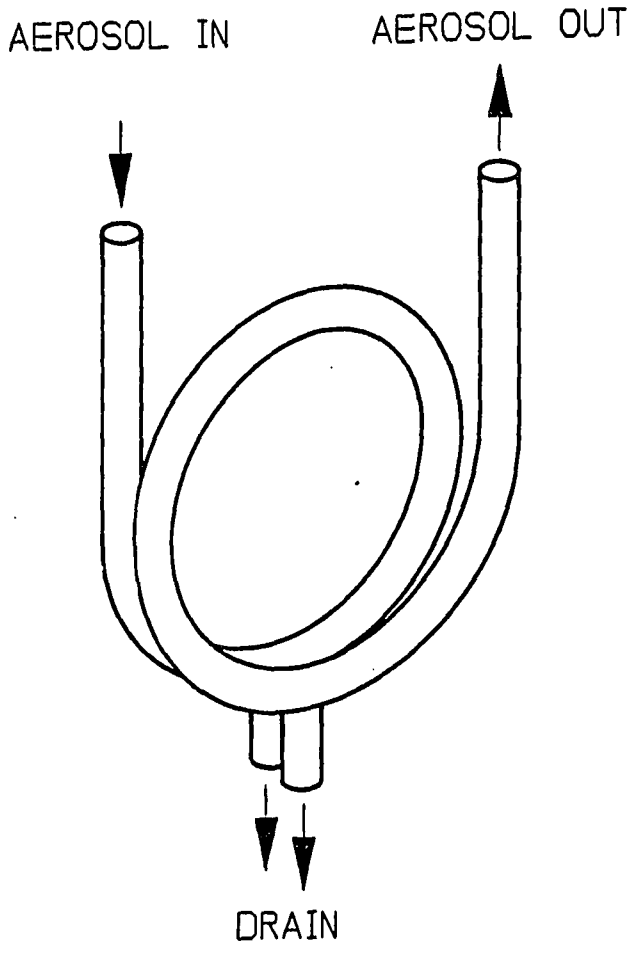

Figure 2. Double-looped cryocondenser.

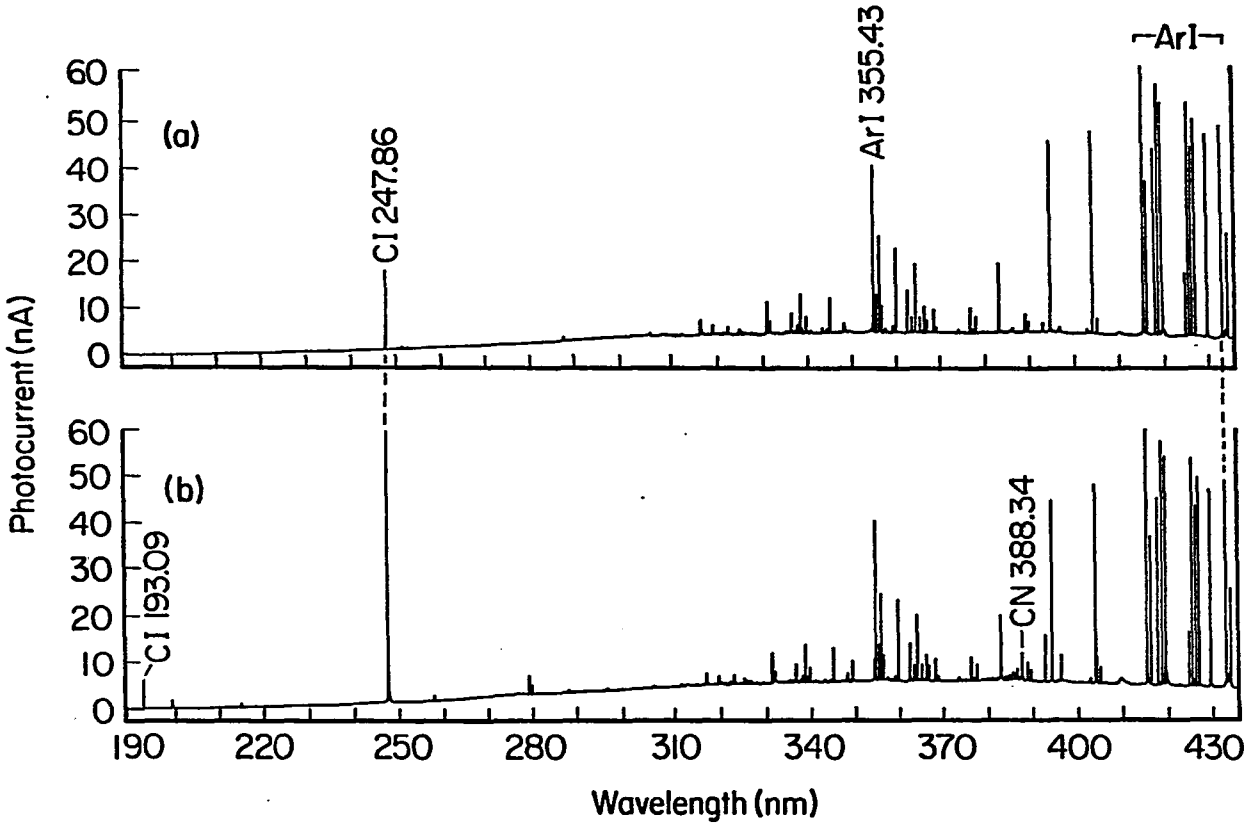

Figure 3. Background scans with nebulization of water (a) and methanol (b). The cryocondenser was used when the methanol spectrum was acquired. Forward power was 1.25 kW. A quartz torch extension was used. Wavelengths lower than 240 nm did not efficiently pass through the extension.

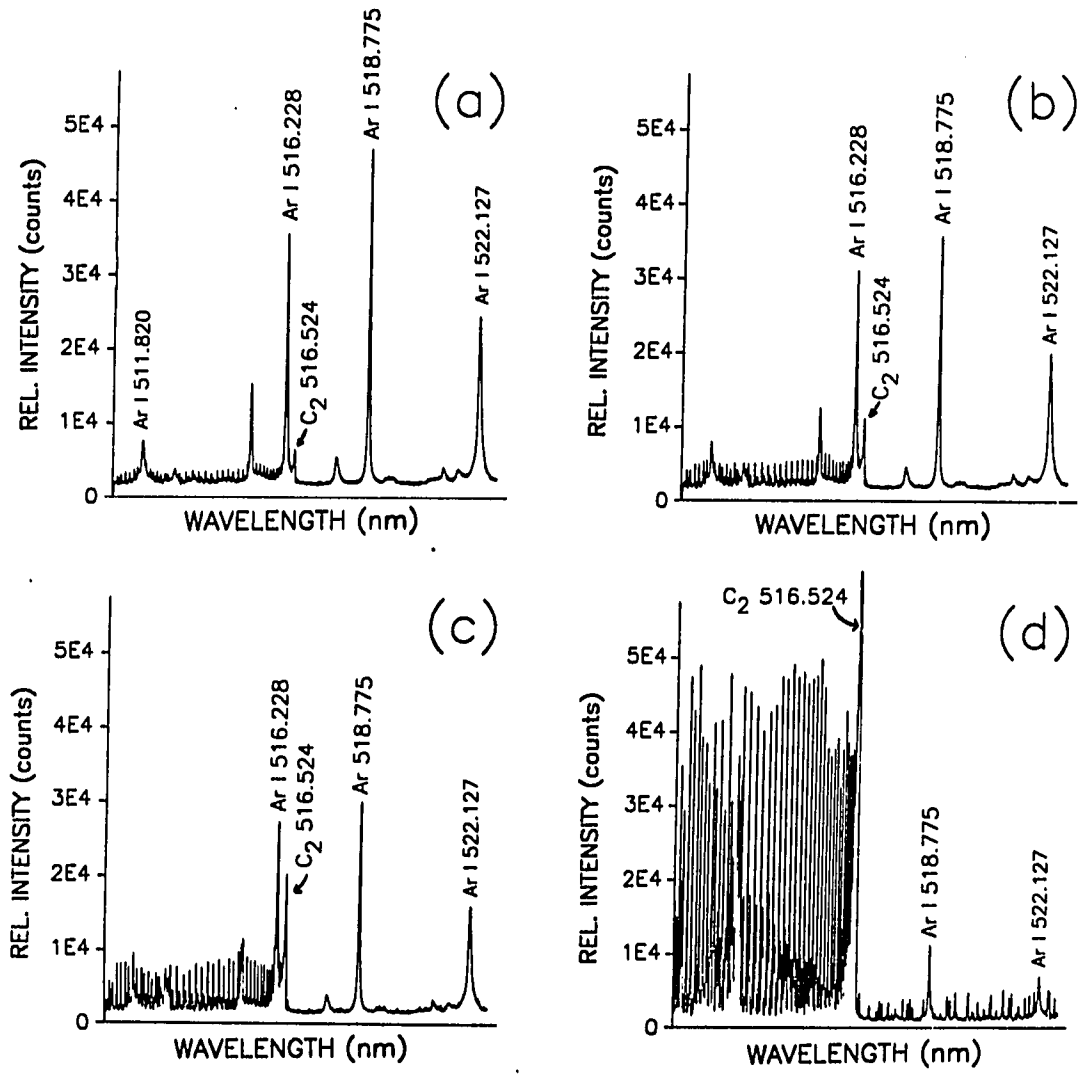

Figure 4. Emission in the C_2 516.524 nm region when methanol was nebulized, showing the effects of the heater temperature and cryocondenser temperature on C_2 and Ar I emission. The primary condenser was maintained at -10 °C in each case. Conditions were: (a) heater at +80 °C, cryocondenser at -80 °C, (b) heater at +25 °C, cryocondenser at -80 °C, (c) heater at +80 °C, condenser at -10 °C, (d) heater at +25 °C, condenser at -10 °C. The offscale C_2 bandhead in (d) reached a maximum intensity of 108,000 counts.

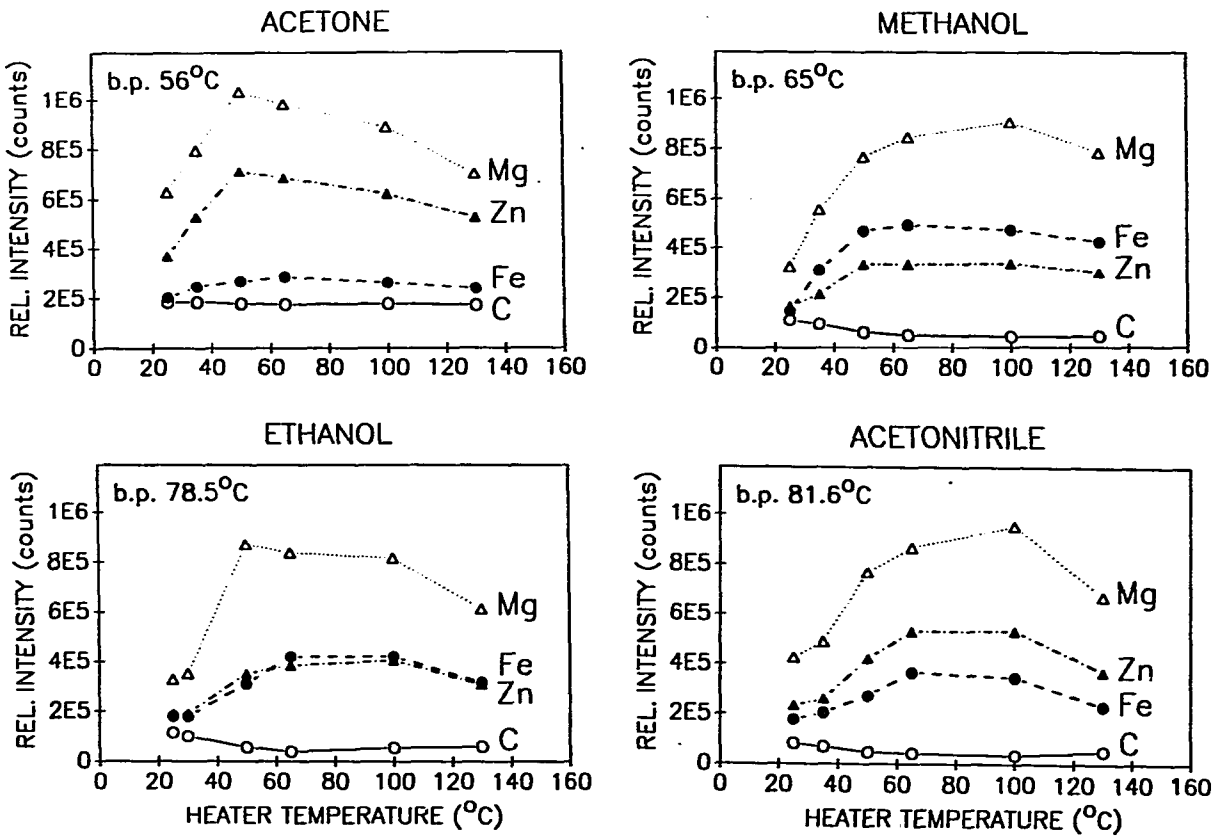

Figure 5. Emission from C I 258.29 nm, Mg II 279.81 nm, Fe II 259.94 nm, and Zn I 213.86 nm as a function of heater temperature for four solvents. Mg intensity data were collected with a 9 s integration time. A 200 s total integration time was used for all other lines. The cryocondenser was at -80 °C for all of these data.

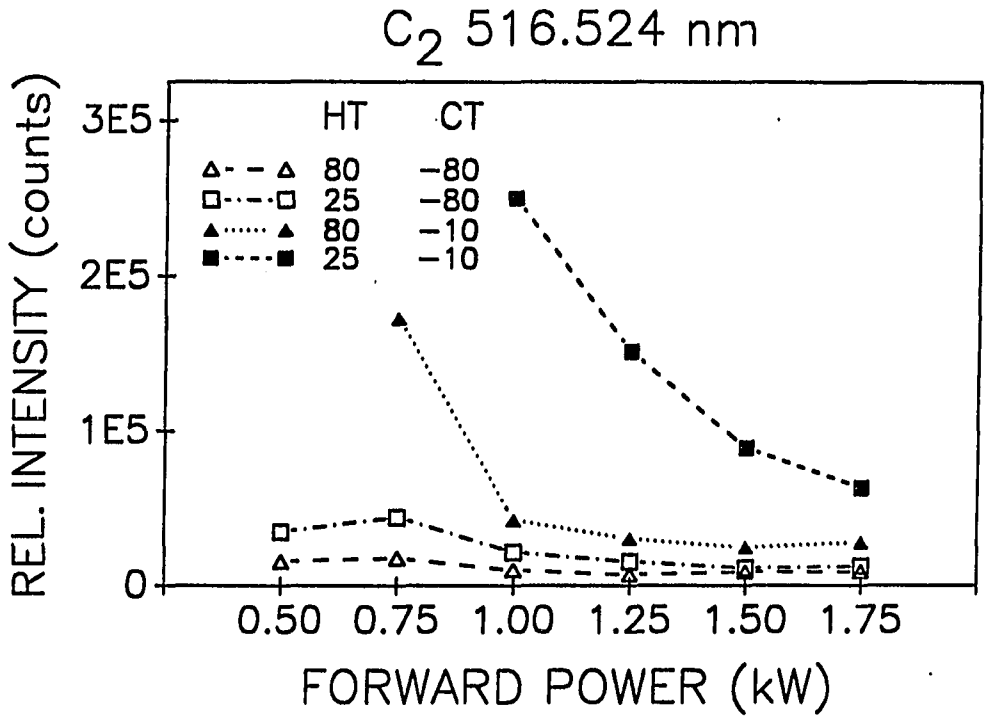

Figure 6. Emission from C_2 when methanol was nebulized as a function of forward power for several combinations of heater and condenser temperature. HT is the heater temperature used. CT is the final condenser temperature before the aerosol enters the plasma.

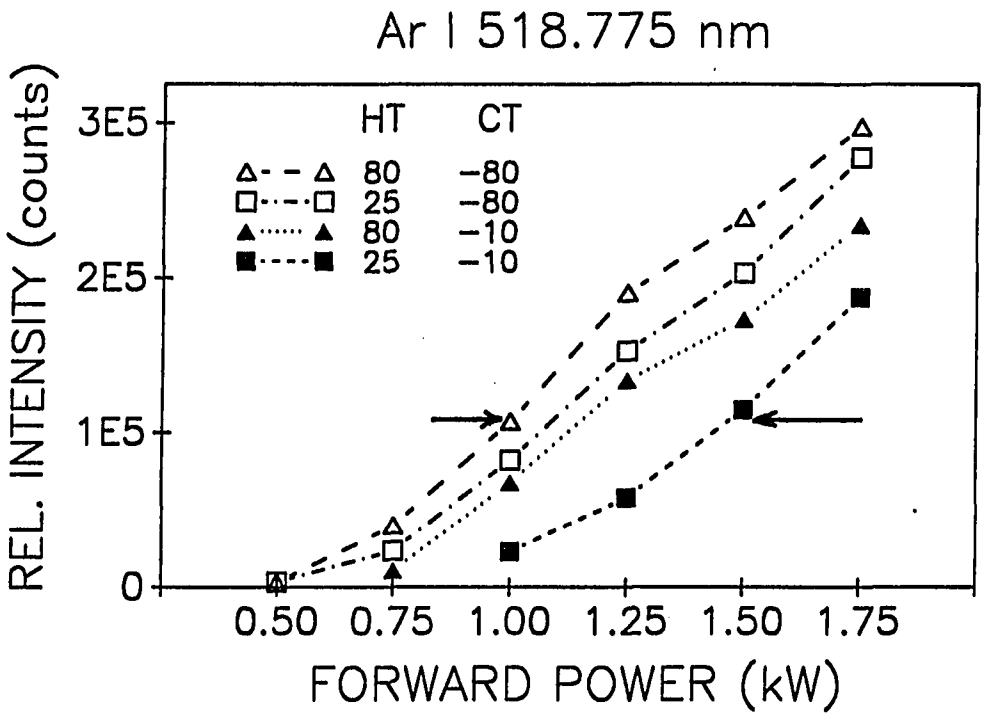

Figure 7. Ar I emission when methanol was nebulized as a function of forward power for several combinations of heater and condenser temperature. HT refers to the heater temperature used. CT is the final condenser temperature before the aerosol enters the plasma. Arrows indicate the ≈ 0.5 kW displacement between the first and last curves.

SECTION II.

DIRECT INJECTION NEBULIZATION FOR INDUCTIVELY COUPLED PLASMA MASS SPECTROMETRY

Introduction

Analysis of liquid samples by inductively coupled plasma mass spectrometry (ICP-MS) usually involves nebulizing the sample into a spray chamber, followed by injection of a fraction of the resulting aerosol into the plasma. This procedure is fraught with deficiencies. For many analyses more time is spent rinsing the nebulizer and spray chamber between samples than is spent measuring the analyte. Determination of volatile elements such as Hg can be difficult because of severe memory effects arising from the spray chamber and transfer tubing. Poor analyte transport efficiency degrades sensitivity and detection limits. Finally, some of the signal imprecision and drift in ICP-MS is likely due to noise originating in the sample introduction system.

An alternative sample nebulization method which did not employ a spray chamber was demonstrated previously for inductively coupled plasma atomic emission spectroscopy (ICP-AES). A microconcentric pneumatic nebulizer, termed a direct injection nebulizer (DIN), was constructed inside the injector tube of the torch. The DIN reduced analyte memory effects and eliminated sample transport losses.

Furthermore, the low dead volume DIN resulted in quicker times to introduce and rinse out samples and reduced peak broadening for flow injection analysis (1-3).

This paper describes a new DIN which is simpler to build and is physically more robust than the original one. In addition, the sample and solvent do not contact any metal surfaces, allowing the determination of trace metals without contamination from the pump or transfer tubing. A gas displacement pump (GDP) provides an inexpensive, metal-free, pulseless, quick-response, high pressure sample delivery pump for the DIN. Analytical figures of merit for the DIN with ICP-MS are reported. The effects caused by a spray chamber and aerosol desolvation on nebulizer performance are also studied.

Experimental

DIN assembly

The new DIN (Figure 1) incorporated several modifications of the original version (1-3). A stainless steel tube (A, Figure 1, 1.6 mm o.d. X 250 μm i.d. X 1.5 cm long) was used as the nebulizer tip rather than a tapered fused silica capillary tube. The metal tip provided a more precisely sized nebulizer orifice and made the entire nebulizer more robust. The nebulizer tip was cemented directly into an alumina tube (B, Figure 1, 3.25 mm o.d. X 1.62 mm i.d.) which supported the nebulizer and provided a conduit for the nebulizer gas. The sample was transported from the flow injection valve to the nebulizer tip

inside a 1 m length of 50 μm i.d. X 200 μm o.d. fused silica capillary tubing (C, Figure 1). The position of this fused silica transfer line was adjusted relative to the stainless steel tube to produce a mist which would not wet a surface 10 cm above the nebulizer tip. The best mist was obtained when the liquid transfer line extended approximately 100 μm beyond the stainless steel nebulizer tube. The end of the transfer tube was cut squarely to avoid large droplets in the mist. No special procedures to center the transfer line were necessary. The dead volume of the transfer line was approximately 2 μL.

The sensitivity obtained with the DIN depended critically on the position of the nebulizer and torch. The DIN was positioned so that the stainless steel nebulizer tube extended 1 mm past the end of the injector tube (D, Figure 1). As shown in Figure 2, the tip of the DIN was flush with the middle tube of the ICP torch. The middle tube of the ICP torch was approximately even with the bottom turn of the load coil. At this position, the DIN was as close to the base of the plasma as possible without being melted.

(Caution: Never look directly down the axis of the DIN during operation. The high gas pressure could drive the nebulizer tip out of the alumina support at high velocity.)

Gas displacement pump

Transport of liquid through the thin (50 μm i.d.) transfer line required a back pressure of nearly 1500 psi. A metal-free gas displacement pump (GDP) (Figure 2) consisting of a well-regulated

pressurized argon source, a carrier solvent reservoir, and a transfer line from the reservoir to the flow injection valve was constructed to transport the sample to the DIN. A compressed argon cylinder and gas regulator (A, Figure 2) were connected to the carrier solvent reservoir (B, Figure 2) to provide the necessary pressure. The solvent reservoir was constructed from 6.3 mm (0.25 in.) o.d. teflon-lined stainless steel tubing (Alltech Associates) and was filled with high purity 2% nitric acid in deionized distilled water. A length of 6.3 mm stainless steel tubing and a pressure relief valve were connected between the gas regulator and the liquid reservoir so that the reservoir could be quickly and safely depressurized prior to filling.

The GDP reservoir had an internal volume of approximately 45 ml, which lasted approximately 6 hours. Using a larger pump reservoir would allow the DIN to be operated for longer uninterrupted periods. The pump was located at the gas cylinder manifold. The solvent stream was transported to the flow injection valve through a 10 m length of tefzel tubing (1.62 mm o.d. X 0.5 mm i.d.).

The GDP reservoir was filled by depressurizing the reservoir using the relief valve, disconnecting the tefzel transfer tubing from the flow injection valve, and then refilling the transfer line and pump reservoir with 2% nitric acid from a syringe. Care was taken to exclude large gas bubbles from the pump reservoir and transfer line because they extinguished the plasma. After the reservoir was filled, the sample transfer line was reattached to the flow injection valve,

the relief valve was closed, and the GDP repressurized. The entire refilling process took about 10 minutes.

The liquid flow rate (usually ~ 120 μL min^{-1}) was optimized by adjusting the gas regulator to vary the pressure applied to the GDP reservoir. Although the GDP flow rate could be controlled precisely, the value for the liquid flow rate could be determined only approximately. To determine the flow rate, liquid was pumped through the DIN at a known flow rate using a liquid chromatography pump (Model 2010, Varian Associates). The back pressure generated was monitored and the same pressure was applied to the GDP to give a similar liquid flow rate. Usually the GDP pressure was adjusted to maximize analyte signal, so accurate measurement of the actual flow rate was not necessary. For experiments where the sample flow rate needed to be known accurately (Figure 3) the liquid chromatography pump was used.

(Caution: The pump materials must safely withstand the high pressures of the GDP. It is important to verify that the maximum allowable working pressure is not exceeded for the dimensions of materials used. Note that the maximum allowable working pressure for tefzel tubing varies from solvent to solvent.)

Flow injection valve

A high-pressure, six port, metal-free flow injection valve (Rheodyne #9125) was used for sample introduction (C, Figure 2). A suction adaptor was available to provide a completely metal-free system. The fused silica capillary from the DIN was inserted as far

as possible into the exit port of the flow injection valve. A vespel ferrule having a 0.3 mm hole was used to secure the fused silica capillary into the flow injection valve. Various sample loops were made from tefzel tubing (0.5 mm i.d. x 1.6 mm o.d.). The loop size was chosen depending upon the time required for the measurement. For rapid measurements a 20 μl loop gave a steady-state signal for 3 to 4 seconds; a 500 μl loop produced a steady-state signal for about 4 minutes. After the measurements were completed at a steady-state signal, the valve was switched to the LOAD position. The sample loop was then manually rinsed with 2% nitric acid before the next sample was injected. This rinse-out procedure was much faster than rinsing the sample loop with only the 120 μl min^{-1} solvent flow.

Spray chamber and desolvation apparatus

A pyrex spray chamber and a desolvation apparatus, similar to that used with an ultrasonic nebulizer (Figure 4 of reference 4), was constructed to investigate the effects of a spray chamber and desolvation on the performance of the nebulizer. A teflon collar held the nebulizer so that its metal tip protruded about 1 mm into the spray chamber. Since waste liquid was generated much more slowly than with conventional nebulizers, the waste was collected using a stoppered 1 foot length of 0.5 inch tygon tubing. A make-up gas flow was added through the spray chamber so the analyte signal could be optimized independently from the nebulizer gas flow rate.

Precision studies

For all precision measurements a single solution containing 0.3 ppm Cr and 0.1 ppm Mn was used. The high analyte concentrations were selected to ensure that the precision was determined by the stability of the instrument and was not limited by counting statistics. Three masses (m/z= 52, 53, 55) were monitored by peak hopping in the multielement mode. For the long-term study, data were collected for 1 hour using a 10 second measurement time and a 20 ms dwell time. A 2.5 mL sample loop was used to provide steady-state signal for an extended period. This loop was refilled twice during each experiment. Short-term precision was measured using a 5 second measurement time and a 20 ms dwell time over a three minute period. For both sets of studies only one m/z position per peak was monitored.

Instrument operation

A standard nickel sampling cone eroded rapidly when water was nebulized through the DIN, possibly due to the high oxygen level in the plasma from the nebulized water. The nickel cone was replaced by a copper one, which tolerated nitric acid solutions for at least several months and was still in use at the time this paper was written. Solutions of 1% hydrochloric acid did erode the copper sampling cone and were avoided. The standard nickel skimmer was not adversely affected by the DIN and was used for all experiments.

In addition to changing the sampling cone, it was necessary to stop the liquid flow to the DIN during plasma ignition. The liquid

flow was shut off by putting the flow injection valve in a position intermediate between LOAD and INJECT. The liquid pressure behind the flow injection valve remained constant while the flow was interrupted when the GDP was utilized. When an HPLC pump was used, the liquid pressure built up behind the valve, causing a surge when the liquid flow was initiated. After starting the plasma the valve was switched to the LOAD position to nebulize the carrier liquid directly into the plasma. It was not necessary to increase the liquid flow rate slowly after starting the plasma (1).

A rather high auxiliary gas flow rate (Table I) kept the plasma away from the DIN tip and increased the analyte signal. A make-up gas flow was added through the injector tube of the ICP torch so that the total gas flow into the axial channel could be adjusted independently of the nebulizer gas flow to optimize the analyte signal. Other plasma operating conditions are listed in Table I. When detection limits were evaluated a 5 s measurement time was used to integrate the steady-state signal from a 20 μL sample loop. The sample injection was synchronized with data acquisition so that the 5 s measurement time spanned the sample pulse. The detection limit was defined as the analyte concentration necessary to yield a net signal equivalent to three times the standard deviation of the background.

Solvents and standards

Iodine solutions were prepared from a sodium iodate (Aldrich Chemical) stock solution (1000 ppm I). All other solutions were

prepared by diluting 1000 ppm standards (Fisher) with a 2% solution of nitric acid (Ultrex II Ultrapure Reagent Grade J.T. Baker) in distilled deionized water (18 MΩ Barnstead). The carrier solvent in the GDP was 2% nitric acid. Other chemicals used were reagent grade.

Results and Discussion

Nebulizer and ICP characteristics

Compared with conventional pneumatic nebulizers, the DIN produced a relatively intense conically shaped aerosol. Very few large droplets were observed either by visual inspection or from still photographs of the DIN aerosol. Calculations (1) showed that the nebulized aerosol left the DIN at a velocity of ~ 120 m sec^{-1}. Although the aerosol was certainly slowed considerably when it entered the more slowly moving plasma, the momentum imparted by the high injection velocity tended to keep the aerosol in a tight plume. Since the nebulizer tip was placed only a few mm from the base of the plasma, the aerosol still had a small cross-sectional area when it entered the plasma, ensuring that nearly all the aerosol was injected into the axial channel. Evidence for this was observed visually when solutions containing 1000 ppm sodium were nebulized. With the DIN, sodium emission was visible only in the axial channel of the plasma. For other nebulizers, sodium emission, although still primarily in the axial channel, was observed around the edges of the plasma as well. For the DIN, nebulized organic solvents also passed directly through

the axial channel with little or no green emission visible near the walls of the torch.

Like most pneumatic nebulizers, the DIN hissed slightly. The hissing sound became quite loud when the plasma was started and liquids were nebulized. No visible fluctuations were observed in the plasma, but generally the analyte ion intensity was greater when the hissing sound diminished. Although the hissing never ceased completely, it was minimized somewhat at higher auxiliary gas flow. The hissing could have been due to the shattering of aerosol droplets in the hot plasma. Use of a DIN with a teflon nebulizer tip instead of stainless steel also produced the hissing, demonstrating that this curious sound was not due to the proximity of metal to the plasma.

Effect of sample flow rate

The sample flow rate affected analyte signal as shown in Figure 3 for Li. Normalized curves obtained for Rb, Rh, and U were nearly identical to Figure 3 except that the loss of U signal was less severe at liquid flow rates above 150 μl min^{-1}. The optimum flow rate for each element was around 120 μl min^{-1}, which was nearly identical to the flow rate found to give the best signal to noise ratio for a DIN with ICP-AES (2). However, in the present work, the signal decreased markedly as the liquid flow rate increased past 120 μl min^{-1}, which could have been caused by solvent loading effects or changes in aerosol droplet size distribution. In contrast, for ICP-AES (with the old DIN) the signal increased with flow rate until about 160 μl min^{-1},

after which the signal intensity leveled off with increasing sample flow rate (1).

The liquid flow rate curves were very nearly linear for flow rates between 30 μl min^{-1} and 120 μl min^{-1}. For example, the correlation coefficient for a line drawn through the five points on the left of Figure 3 was 0.998. In this region, the sample liquid flow rate determined both the mass flow rate of analyte into the plasma and the analyte signal. This observation suggested the alluring possibility of generating calibration curves from only one standard by simply varying the liquid flow rate. The samples could then be analyzed while the liquid flow rate was held in the middle of the linear portion of the curve, say 75 μl min^{-1} in Figure 3. For the data presented in this paper, the liquid flow rate was kept at 120 μl min^{-1}.

Washout characteristics

At the optimum nebulizer flow rate (120 μl min^{-1}), the analyte signal reached a steady-state level only 3 seconds after sample introduction. The sample transfer line had a volume of 2 μl and was swept out about once each second. Thus, a steady state signal was reached within three volume rinsings.

The rinse-out profiles for 1 ppm solutions of Hg and I are shown in Figure 4. In each case the analyte signal was at a steady-state for at least one minute before the rinse-out was initiated. At time zero the flow injection valve was switched from the INJECT position to

the LOAD position. In the LOAD position the 2% nitric acid flowed directly from the GDP to the DIN, rinsing the nebulizer in the process. The drop in signal at time zero, particularly noticeable for Hg, occurred because the liquid flow to the nebulizer was momentarily interrupted as the valve was switched. The signal then briefly increased as the sample remaining in the transfer line was nebulized, followed by rapid rinse-out to the background level (~ 100 counts s^{-1}). The rinse-out time is somewhat dependent upon the carrier solvent. For example, when water was used as the carrier solvent instead of 2% nitric acid the rinse-out time for Hg nearly doubled.

With conventional nebulizers Hg and I normally exhibit severe memory effects (5,6). In our experience, more than 10 minutes was required to rinse out Hg and I signals to 0.1% of their steady-state values. When using the DIN with Hg, I, or any of the elements listed in Table II, the rinse-out time was 15 s or less. Thus, the DIN should facilitate the determination of difficult elements such as Hg and improve sample throughput considerably for all analytes.

In Figure 4 the background levels for Hg and I were around 100 counts s^{-1}. Typically, when the DIN was used the background count rate was between 40 and 100 counts sec^{-1}, compared to 10 to 20 counts sec^{-1} with a conventional nebulizer. In the case of Hg the background was not due to Hg memory because the count rates for both the minor Hg isotope at m/z = 196 and the most abundant isotope at m/z = 202 were equivalent and there was no Pt contamination. Fortunately the detection limits were not significantly degraded by the higher

background because the standard deviation of the background was low (typically < 5 counts sec^{-1}).

Figure 5 illustrates determination of Hg at the part per billion level in aqueous solution. Four 200 μl volumes of 1 $\mu g\ L^{-1}$ Hg were nebulized. In order to improve counting statistics a 10 second measurement time was employed. The precision for both the background and the Hg signal was at the counting statistics limit. A fifth injection of 2% nitric acid blank showed a small spike approximately at the detection limit for Hg. An additional blank injection (not shown) showed no spike, indicating that the previous spike was probably due to a small amount of residual Hg left in the valve from the Hg samples. Use of a flow injection valve with a smaller dead volume and thorough rinsing of the loop and valve between injections should minimize potential carryover.

Sensitivity and detection limits

The data in Table II were collected under the same conditions for all elements except that a different photon stop potential was used for each of the three mass ranges, as indicated in Table I. The general range of relative detection limits was 0.01 to 0.1 $\mu g\ L^{-1}$, which was comparable to relative detection limits found with this ICP-MS instrument with conventional pneumatic nebulizers. The absolute detection limits when using the DIN were roughly ten times better than those found previously for this ICP-MS instrument when using a pneumatic nebulizer. The improvement in absolute detection limits

occurred primarily because the sample consumption was an order of magnitude lower than that for conventional nebulizers.

Precision with DIN

A conventional nebulizer generally requires a spray chamber. Turbulence during nebulization (7) and pressure pulses as waste drains from the walls of the spray chamber could contribute to imprecision in the analytical signal (8). To investigate the effect of a spray chamber on signal precision, measurements were made using the microconcentric nebulizer positioned either at the base of the plasma (DIN) or in a spray chamber. Special conditions employed to maximize the signal for analyte ions when the microconcentric nebulizer was used with a spray chamber are listed in Table III. A desolvation apparatus was not used during these precision measurements.

The data in Table IV illustrated typical precision values for both the short term (3 minute) and the long term (1 hour) when the identical microconcentric nebulizer was positioned in either of two configurations. The data were presented in percent relative standard deviation (RSD, 1 σ). The RSDs were the means of those obtained in three separate experiments. The count rates were nearly identical whether the nebulizer was positioned in a spray chamber or used as a direct injection nebulizer at the base of the plasma, even though part of the sample was not transported into the plasma when the spray chamber was used. This apparent discrepancy may be due to one or more of the following effects: a) a change in the plasma caused by the DIN

itself; b) the necessarily different operating conditions used when the nebulizer was located in a spray chamber (Table III); or c) opposing effects related to changes in solvent loading and droplet size distribution when the spray chamber was used.

When the microconcentric nebulizer was used at the base of the plasma the precision of the $^{52}Cr^{+}$ count rate was 0.4% RSD for short term measurements and was 1.2% RSD for long term measurements (Table IV). These precision values are typical of those obtained for other elements when the DIN was used, and are at least 4 times superior to those obtained on this ICP-MS instrument using conventional nebulizers. When the identical nebulizer was positioned in a spray chamber, however, the precision was poorer for both the short and long term measurements. In fact, the precision for the microconcentric nebulizer in a spray chamber was fairly typical of values obtained by a number of workers using conventional pneumatic nebulizers with ICP-MS (10,11). Thus, the four-fold improvement in precision with the nebulizer at the base of the plasma is likely the result of eliminating the spray chamber and aerosol transfer tubing and is not due to nebulizer construction or pulseless sample delivery with the GDP. The fundamental reasons for the striking and unexpected improvements in precision found in the absence of a spray chamber are intriguing and merit further investigation.

ICP-MS workers often use internal standardization and isotope dilution to improve accuracy and precision. As shown in Table IV, internal standardization offered no improvement in precision for

short-term measurements and only a modest improvement for long term measurements. The precision for the internal standard measurement was better with the DIN at the base of the plasma, but the precision of the isotope ratio measurements was essentially the same for either nebulizer configuration, for reasons that are again unclear.

Oxide ions and desolvation

Because the DIN was adjacent to the plasma, the nebulized solvent could not be removed. Thus, polyatomic ions derived from solvent molecules caused worse spectral interferences with the DIN. Under conditions which yielded the optimum M^+ signal (Table I), the ratio MO^+/M^+ for refractory metal oxides such as La and U was 50% to 100%.

To reduce the metal oxide interference the sampling position was changed to 26 mm from the load coil, 6 mm downstream from the position that yielded the highest M^+ signal. In addition a slightly lower make-up gas flow rate (0.10 L min^{-1}) was used. These changes reduced the MO^+/M^+ ratio to around 7% (Table V) but cut the M^+ signal by 20% to 50%. For aqueous solvent, further adjustments to the sampling position or make-up gas flow rate reduced the MO^+/M^+ ratio to 4%, but with 90% signal loss for La^+ and U^+.

Although the nebulization of water led to high oxide ion levels when the DIN was used, accurate corrections were possible because the count rate for MO^+ was highly precise (~ 0.5% RSD). Still, it was desirable to attenuate the interference as much as possible. Two methods were tested to mitigate refractory oxide ions. First, ethanol

was added to the sample solution at 20%. Upon nebulization of the ethanol:water solution, the hissing sound (see above) moderated and the M^+ count rate nearly doubled (Table V). The MO^+/M^+ ratios were reduced to 2% - 2.5%, values typically observed for these oxides on this type of instrument with a conventional pneumatic nebulizer (12). Thus, addition of ethanol to the sample solution both reduced the MO^+/M^+ ratio and increased the analyte signal. The plasma tolerated ethanol surprisingly well. Very little green C_2 emission was visible from the plasma until the fraction of ethanol exceeded 50%. Nebulization of absolute ethanol did not extinguish the plasma, but a considerable amount of green emission was visible, and carbon deposited on the sampling cone.

With 20% ethanol in water an excess of oxygen compared to carbon was present in the plasma. Others have shown that an excess of oxygen (usually as O_2) prevented carbon deposition on the sampling cone when organic solvents were nebulized (13,14). In addition, the DIN injected the sample directly into the base of the plasma, preventing organic solvent vapors from flowing around the base of the plasma and reaching the induction region, where solvent-derived organic species could quench the plasma (15).

The second approach to attenuating oxide ions was to put the nebulizer in a spray chamber and desolvate the aerosol. Upon leaving the spray chamber the aerosol was heated to 140 ^{o}C and the aerosol stream was then cooled in an ice water condenser to remove a portion of the aqueous solvent (4). As shown in Table V, use of a spray

chamber and desolvation yielded the highest count rates for M^+ and the lowest oxide ratios. Of course, rinse-out time and precision were sacrificed, and memory-prone elements such as Hg and I could not be determined with this approach. When the DIN was placed in a spray chamber and the aerosol was desolvated, the MO^+/M^+ ratios were reduced to levels of 0.7% to 1.6%, which are typical of those found when other nebulizers (i.e., pneumatic and ultrasonic) were used with desolvation for ICP-MS (16-18).

Matrix effects

The i.d. of the fused silica line (C, Figure 1) was only 50 μm, and the annular space between the fused silica line and the stainless steel tube (A, Figure 1) was only 25 μm wide. Despite these small limiting orifices, the DIN resisted clogging by samples with high levels of dissolved solids. For example, a seawater sample was nebulized for thirty seconds without clogging the nebulizer or sampling cone. Generally, deposits accumulated on the mass spectrometer sampling cone before they became noticeable on the DIN. However, when solutions with 1% salt content were continuously nebulized for about five minutes the central channel of the plasma began to be skewed. This skewing was presumably due to salt build-up on the tip of the DIN. Nebulizing 2% nitric acid for approximately 1 minute removed the deposit and the axial channel was once more aligned properly. In general, with solutions containing high salt content a small sample loop volume (e.g., 20 μl) prevented salt deposits on the

sampling orifice and the tip of the DIN, as was previously observed with flow injection with ICP-MS (19-21). Also, by increasing the flow rate of make-up gas to 0.5 L min^{-1} the skewing problem was eliminated.

Figure 6 shows data from 20 μl injections of solutions containing both 10 ppb Tl and Hg with 0%, 0.1%, and 1.0% Na added as sodium nitrate. In Figure 6a, a 0.1% Na matrix produced a 40% loss in Tl^+ signal; a 1% Na matrix reduced the Tl^+ signal by 65%. These matrix effects are comparable to or slightly more severe than with conventional nebulizers (22-28).

Figure 6 also shows that Na suppressed the Tl^+ signal more than the Hg^+ signal. Further experiments with gold showed that the Au^+ signal was lost less severely than the Tl^+ signal, but more than the Hg^+ signal. For these analytes of similar mass, the extent of suppression decreased in the order Tl > Au > Hg, which was inverse to the order of ionization energy (Tl < Au <Hg). This observation was interesting but is not readily explained. This also illustrated the general caveat that internal standardization should not be assumed to compensate perfectly for matrix effects and should be tested experimentally before use (23). As shown in Figure 6, the signals were recovered after replicate injections, so the matrix effects were not caused by clogging of either the nebulizer or the sampling orifice.

Conclusion

The DIN described in the present work has many potential uses, especially in applications where the sample size is limited. The low dead volume and high nebulization efficiency make it attractive for flow injection ICP-MS, which is a valuable method for analyzing highly concentrated solutions such as urine or brines without blocking the sampling orifice. The ability to detect picogram levels of analyte offers a number of possibilities for detection of trace elements and for stable isotope labelling. Small sample volumes reduce the amount of the isotope spike required for isotope dilution by about an order of magnitude. Use of small volumes is also advantageous when the sample is preconcentrated prior to analysis. The DIN would permit a higher concentration factor because of the smaller volume required for the measurement step. For radioactive samples the DIN would minimize the sample volume to reduce laboratory hazards. Since the sample is completely consumed in the nebulizer, no liquid waste remains for disposal, although solid deposits must still be removed from the sampling cone periodically. The DIN is very attractive for combining LC separations with element-selective detection by ICP-MS. These application experiments, as well as fundamental characterization of the aerosol produced by the DIN, are continuing in our laboratory.

Literature Cited

1. Lawrence, K. E.; Rice, G. W.; Fassel, V. A. Anal. Chem. 1984, 56, 289-292.
2. LaFreniere, K. E.; Rice, G. W.; Fassel, V. A. Spectrochim. Acta, Part B 1985, 40B, 1495-1504.
3. LaFreniere, K. E.; Fassel, V. A.; Eckels, D. E. Anal. Chem. 1987, 59, 879-887.
4. Fassel, V. A.; Bear, B. R.; Spectrochim. Acta, Part B 1986, 41B, 1089-1113.
5. Bushee, D. S. Analyst 1988, 113, 1167-1170.
6. Gray, A. L. Applications of Inductively Coupled Plasma Mass Spectrometry; Chapman and Hall: New York, 1989, p 34.
7. Sharp, B. L. J. Anal. Atom. Spectrom. 1988, 3, 939-963.
8. Browner, R. F.; Boorn, A. W. Anal. Chem. 1984, 56, 875A-888A.
9. Scott, R. H.; Fassel, V. A.; Kniseley, R. N.; Nixon, D. E. Anal. Chem. 1974, 46, 75-80.
10. Houk, R. S.; Thompson, J. J. Mass Spectrom. Rev. 1988, 7, 425-461.
11. Crain, J. S.; Houk, R. S.; Eckels, D. E. Anal. Chem. 1989, 61, 606-612.
12. Lam, J. W. H.; Horlick, G. Spectrochim. Acta, Part B 1990, 45B, in press.
13. Browner, R. F.; Boorn, A. W. Anal. Chem. 1984, 56, 786A-798A.
14. Hausler, D. Spectrochim. Acta, Part B 1987, 42B, 63-73.

15. Boorn, A. W.; Cresser, M. S.; Browner, R. F. Spectrochim. Acta, Part B 1980, 35B, 823-832.

16. Houk, R. S. Anal. Chem. 1986, 58, 97A-105A.

17. Hutton, R. C.; Eaton, A. N. J. Anal. Atom. Spectrom. 1987, 2, 595-598.

18. Zhu, G.; Browner, R. F. J. Anal. Atom. Spectrom. 1988, 3, 781-789.

19. Houk, R. S.; Thompson, J. J. Biomedical Mass Spectrom. 1983, 10, 107-112.

20. Beauchemin, D.; Siu, K. W. M.; Berman, S. S. Anal. Chem. 1988, 60 2587-2590.

21. Hutton, R. C.; Eaton, A. N. J. Anal. Atom. Spectrom. 1988, 3, 547-550.

22. Olivares, J. A.; Houk, R. S. Anal. Chem. 1986, 58, 20-25.

23. Thompson, J. J.; Houk, R. S. Appl. Spectrosc. 1987, 41, 801-806.

24. Kawaguchi, H.; Tanaka, T.; Nakamura, T.; Morishita, M. Anal. Sci. 1987, 3, 305-308.

25. Tan, S. H.; Horlick, G. J. Anal. Atom. Spectrom. 1987, 2, 745-763.

26. Beauchemin, D.; McLaren, J. W.; Berman, S. S. Spectrochim. Acta, Part B 1987, 42B, 467-490.

27. Gillson, G. R.; Douglas, D. J.; Fulford, J. E.; Halligan, K. W.; Tanner, S. D. Anal. Chem. 1988, 60, 1472-1474.

28. Crain, J. S.; Houk, R. S.; Smith, F. G. Spectrochim. Acta, Part B 1988, 43B, 1355-1364.

Table I. Instrument Conditions and Operating Procedures.

ICP-MS	Sciex Elan Model 250
ICP torch	Modified Sciex short torch: Injector tube orifice diam. = 1.75 mm 6 mm o.d. x 4 mm i.d. quartz tee attached at torch base.
Argon flow rates:	
outer	14 L min^{-1}
intermediate	1.5 L min^{-1}
make-up	0.20 L min^{-1} regulated by mass flow controller
DIN nebulizer gas (argon):	
pressure	200 psi
flow rate	1.0 L min^{-1}
Plasma forward power	1.50 kW
Sampling position	On center 20 mm above load coil [a]
Sample liquid flow rate	120 μl min^{-1} [a]
Detector voltage	-4000 V
Ion lens settings:	
Einzel 1 & 3	-19.80 V
plate	-11.00 V
barrel	+5.42 V
photon stop	
m/z < 40	-3.80 V
m/z 50 to 175	-4.96 V
m/z > 175	-6.94 V
Flow injection valve	Rheodyne # 9125 metal-free sample loops constructed from 1/16" tefzel tubing

[a] Unless specified otherwise.

Table II. Sensitivity and Detection Limits for 20 μL Injection Volumes.

ELEMENT	SENSITIVITY (counts s^{-1} ppm^{-1})	DETECTION LIMITS	
		Absolute (pg)	Relative (μg/L)
^{59}Co	1,860,000	0.2	0.009
^{107}Ag	1,010,000	0.2	0.01
^{114}Cd	435,000	1	0.05
^{127}I	320,000	1	0.06
^{192}Os	140,000	2	0.09
^{202}Hg	88,000	2	0.1
^{205}Tl	945,000	0.2	0.01
^{208}Pb	613,000	0.8	0.04
^{238}U	335,000	0.6	0.03

Table III. Conditions for Operating Microconcentric Nebulizer in Spray Chamber.

ICP torch		Fassel-type, injector orifice diameter = 1.5 mm (9)
Argon flow rates:		
	outer	12 L min^{-1}
	intermediate	0.4 L min^{-1}
	make-up	0.6 L min^{-1} (introduced through the spray chamber)
Nebulizer:		
	pressure	200 psi
	flow rate	1.0 L min^{-1}
Sampling position		22 mm above load coil
Plasma forward power		1.25 kW
Spray chamber		Ames Laboratory construction, the type typically used with an ultrasonic nebulizer (4).

Table IV. Precision values (expressed as percent relative standard deviation) for one microconcentric nebulizer used either at the base of the plasma (direct injection mode) or in a spray chamber.

	Short Term RSD (%) (3 minute)		Long Term RSD (%) (1 hour)	
	Direct Injection	Positioned in Spray Chamber	Direct Injection	Positioned in Spray Chamber
COUNT RATE ($^{52}Cr^+$)	0.40	1.7	1.2	5.6
INTERNAL STANDARD ($^{52}Cr^+/^{55}Mn^+$)	0.38	2.0	0.92	3.9
ISOTOPE RATIO ($^{52}Cr^+/^{53}Cr^+$)	0.25	0.28	0.37	0.45

Table V. Comparison of sensitivity and MO^+/M^+ ratios for different nebulizer configurations.

Nebulizer Configuration	Solvent	$^{139}La^+$ sensitivity (counts s^{-1} ppm^{-1})	LaO^+/La^+ (%)	$^{238}U^+$ sensitivity (counts s^{-1} ppm^{-1})	UO^+/U^+ (%)
DIRECT INJECTION[a]	Water	456,000	6.6	312,000	7.2
DIRECT INJECTION[a]	20% Ethanol/ 80% Water	852,000	1.9	588,000	2.5
POSITIONED IN SPRAY CHAMBER, AEROSOL DESOLVATED[b]	Water	1,000,000	1.6	782,000	0.7

[a] Sampling position = 26 mm.

[b] Conditions listed in Table III.

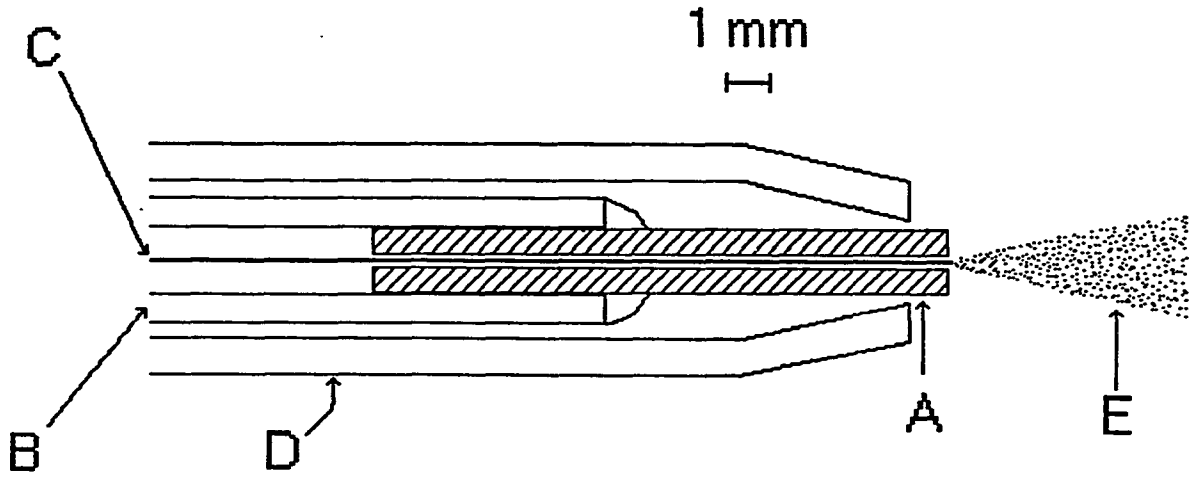

Figure 1. An enlarged view of the direct injection nebulizer (DIN) tip: [A] stainless steel nebulizer tip; [B] ceramic support tube; [C] fused silica sample transfer line; [D] quartz injector tube of torch; [E] nebulized aerosol. The nebulizer tip is cemented to the ceramic tube using epoxy resin. All dimensions, including the aerosol, are to scale except the fused silica capillary which is shown at one-half diameter for clarity.

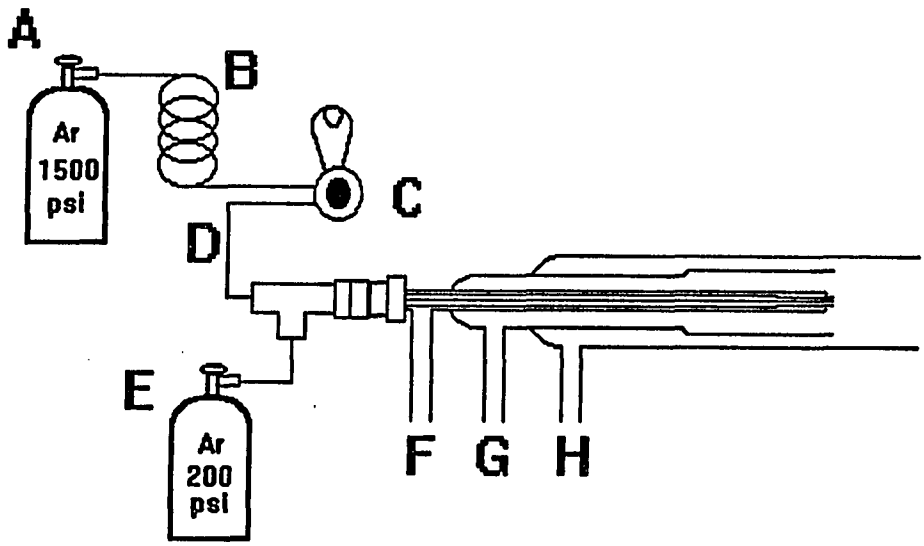

Figure 2. Diagram of the DIN, sample introduction system, and gas displacement pump (GDP): [A] argon supply for GDP (1500 psi); [B] teflon-lined stainless steel tubing used as reservoir for GDP; [C] high-pressure, metal-free flow injection valve; [D] 50 μm i. d. fused silica sample transfer line; [E] nebulizer argon supply (200 psi); [F] make-up injector gas; [G] auxiliary gas; [H] plasma gas.

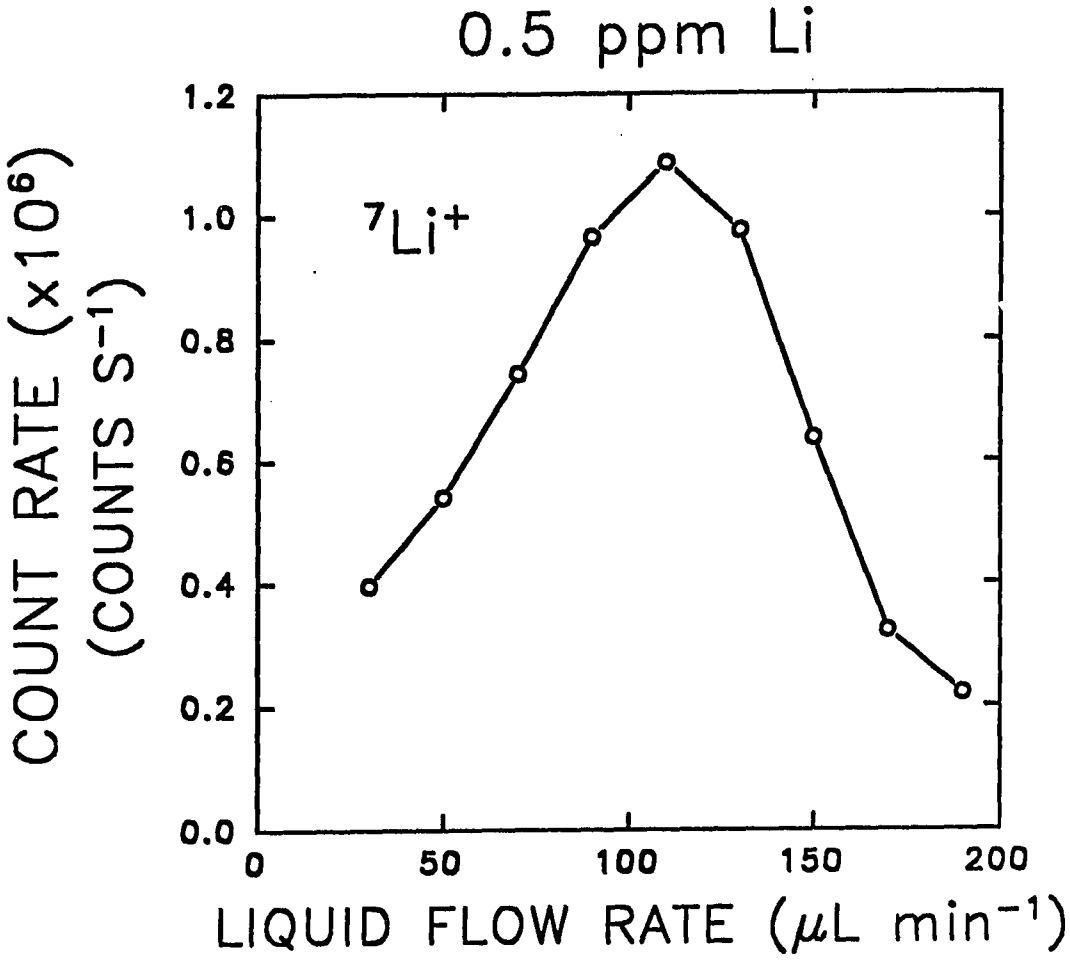

Figure 3. Effect of liquid flow rate on Li^+ signal.

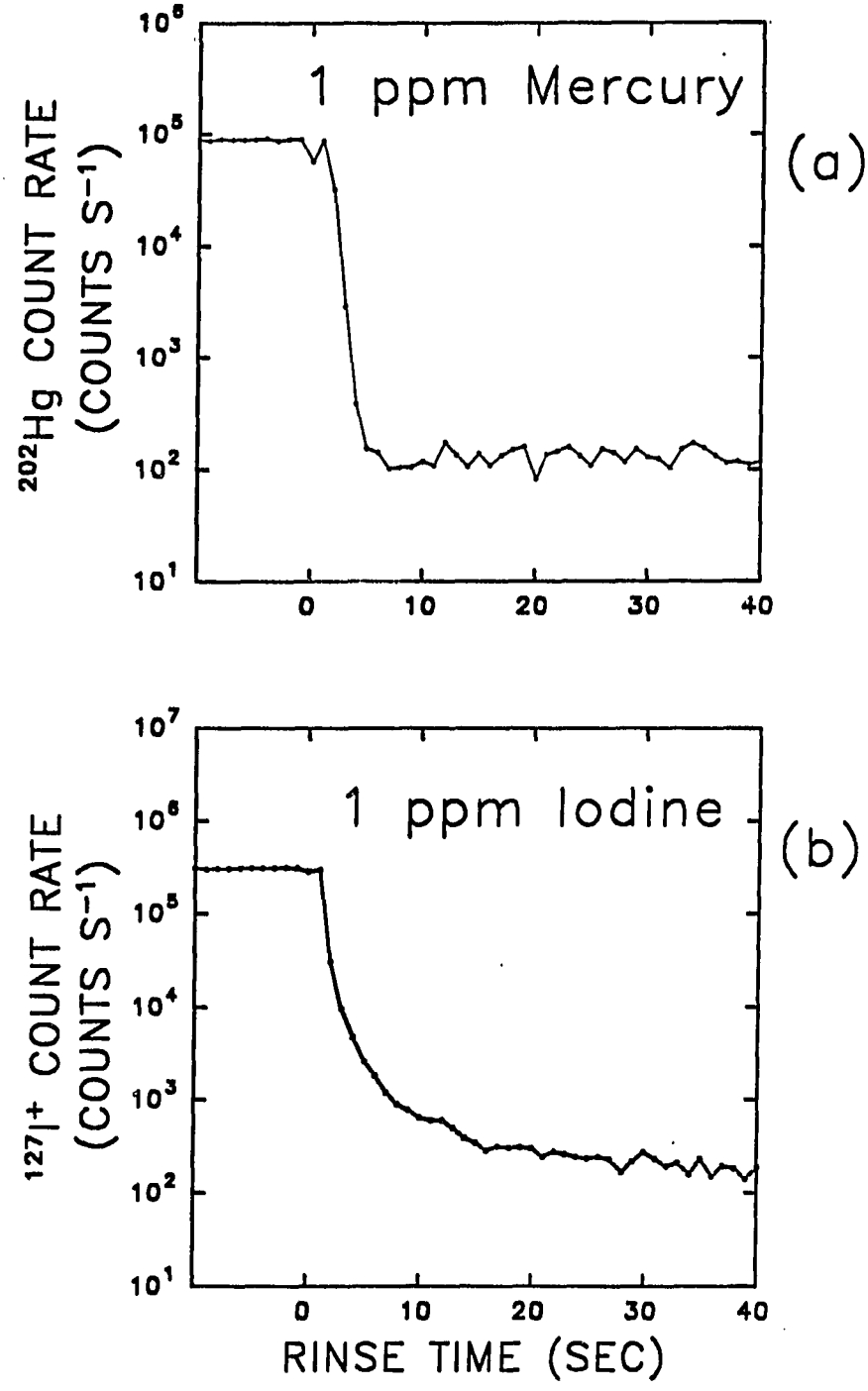

Figure 4. Rinse-out profiles for Hg (a) and I (b), each element at 1 ppm. The sample was removed at time = 0.

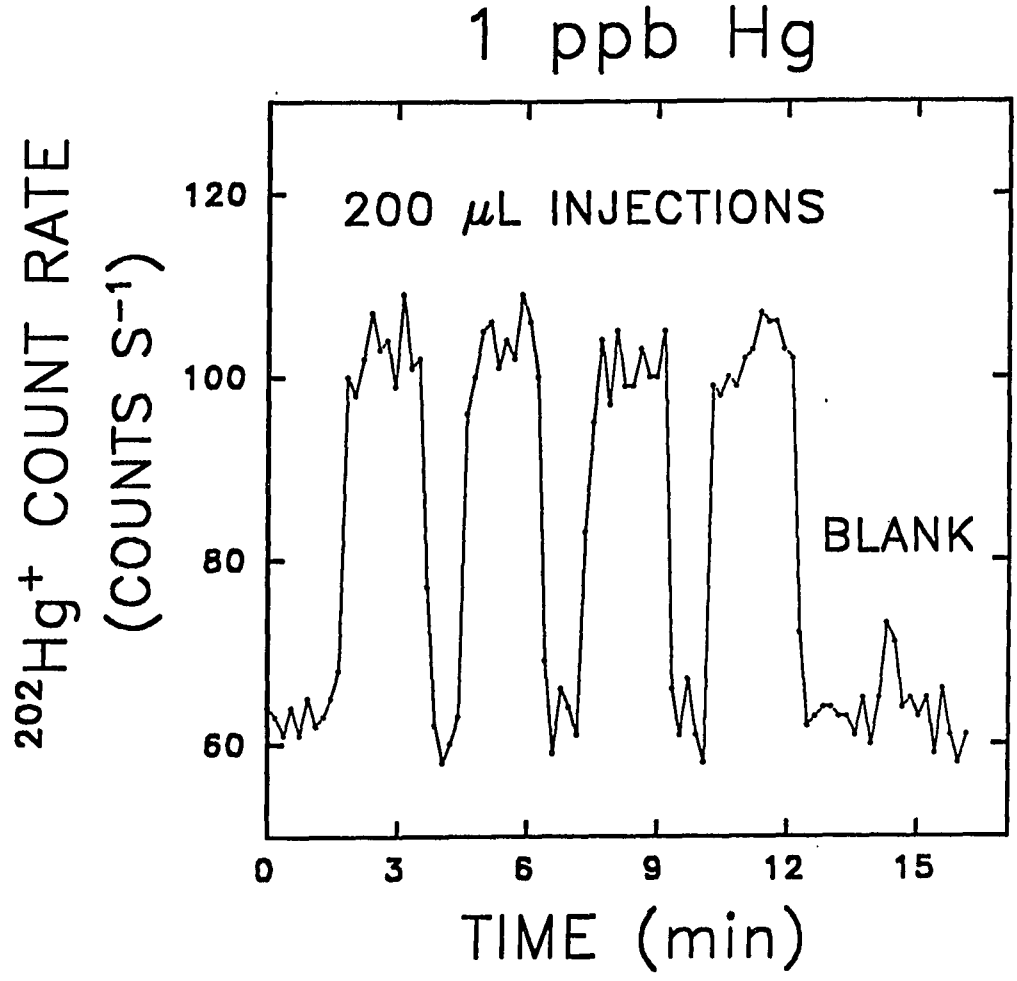

Figure 5. Flow injection and rinse-out for four injections of 200 pg total Hg, followed by one blank injection.

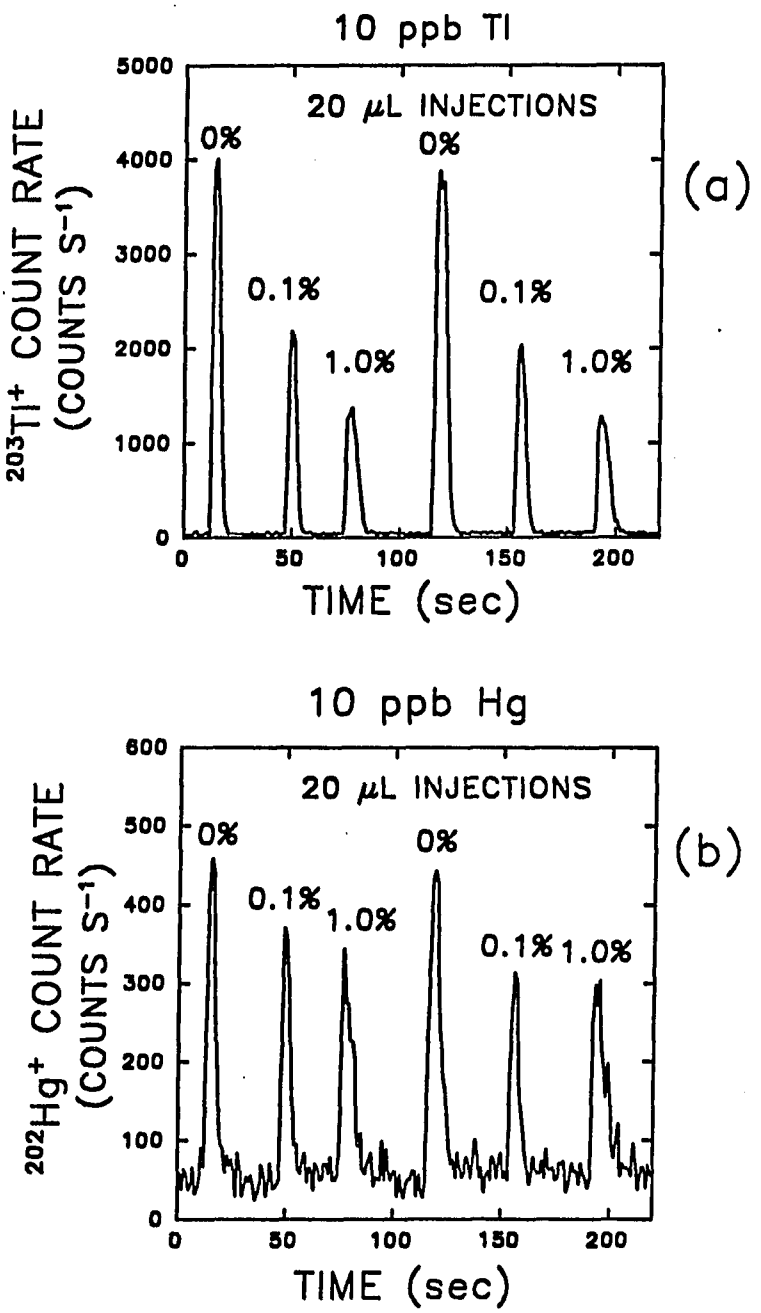

Figure 6. Effect of Na (as $NaNO_3$) on signals for Tl^+ (a) and Hg^+ (b). The percent values indicate the concentration of Na concomitant.

SECTION III.

MEASUREMENTS OF AEROSOL PARTICLE SIZE FROM A DIRECT INJECTION NEBULIZER

Introduction

Recently microconcentric pneumatic nebulizers have been constructed inside a torch used for inductively coupled plasma (ICP) spectrometry. Versions of this device, called a direct injection nebulizer (DIN), have been employed to nebulize samples directly into an ICP for emission (1-4) and mass spectrometric (5-7) analyses. These nebulizers consumed sample solution at a rate of only 100 μL min^{-1}, yet provided good sensitivity, rapid sample rinse times, and low memory effects. Furthermore, the DIN used for ICP-MS gave better precision than conventional nebulizers used with a spray chamber (5).

The DIN was unique because a spray chamber was not required to remove large droplets from the sample aerosol. Previously, others have shown that the analytical signal from an ICP depended on the size of the sample aerosol particles introduced to the plasma and that analyte present in large particles did not improve the signal to background ratio (8). Thus the sample aerosol for ICP spectrometry should contain small particles in a narrow range of sizes. Since the DIN aerosol size distribution was not modified by a spray chamber, it was important to compare the droplet sizes from the DIN to those from

conventional concentric pneumatic nebulizers. This comparison is the basis of the present work.

Experimental

A Meinhard TR-30-C3 glass concentric nebulizer (Meinhard Associates, Santa Ana, CA) was used for comparative purposes because it is commonly used for ICP spectrometry. The DIN was similar to those described previously (5-7). The DIN sample delivery tube was 40 μm i.d. x 144 μm o.d. fused silica. The annular space between the sample tube and the nebulizer gas tube was 15 μm wide. Distilled, deionized water was delivered to the DIN at 100 μL min^{-1} and to the Meinhard nebulizer at either 100 μL min^{-1} or 1000 μL min^{-1} using a liquid chromatography pump (Varian Model 2010). The argon nebulizer gas flow rate was adjusted by varying the back pressure with a gas regulator.

A forward scattering spectrometer probe (FSSP-100, Particle Measuring Systems, Boulder, CO) was used for aerosol characterization. Probe operation was based upon light scattering principles which have been discussed in greater detail elsewhere (9-11). The FSSP used a small fan to draw the nebulized aerosol across a region traversed by a He-Ne laser beam (632.8 nm). The intensity of scattering produced by individual droplets as they passed through the laser depended upon drop size. A photodetector measured the intensity of scattered light. The instrument used a pulse-height analyzer to classify the signal

detected for each droplet into one of 15 channels of equivalvent width.

The instrument had been previously calibrated for several different size ranges, which could be selected via computer control. The size ranges used were 1 to 16 μm, 2 to 32 μm, and 5 to 95 μm. For each aerosol, the range selected was the narrowest which included all the aerosol particles detected by the FSSP. An initial measurement was made on each aerosol using the 5 to 95 μm range to determine the largest particle size in the aerosol. When the DIN was used, no particles larger than 30 μm were detected, so further measurements were made using the 2 to 32 μm range. Similarly, for the aerosol exiting a Scott-type spray chamber no particles over 14 μm were found, so the 1 to 16 μm range was selected. The scales on the horizontal axes in the figures reflect the size range used for data collection. To calculate the mass (volume) distribution of the aerosol, the number of droplets was counted in each of the 15 size classes. These counts were then converted to the corresponding mass percent values.

The aerosol was sampled by holding the end of the nebulizer (or the exit of the spray chamber) in a plane 5 cm from the laser beam. An attempt was made to compensate for possible tomographic effects by moving the nebulizer in a circular orbit (radius ~ 1 cm) within the sampling plane. A 60 s acquisition time was used for all measurements except when the spray chamber was used. The aerosol mass which exited the spray chamber was at least an order of magnitude lower than that

for the DIN. Thus, a 120 s acquisition time was employed to increase the number of particles counted for these measurements.

Results and Discussion

Figure 1a-c compares the aerosol mass distribution produced by a DIN operated at gas flow rates of 0.2, 0.4, and 0.5 L min^{-1}. To achieve these flow rates, the nebulizer gas pressure was adjusted to 100, 150, and 200 psi, respectively. In each case the usual liquid flow rate of 100 μL min^{-1} was used (5-7). Figure 2a shows the mass distribution for an aerosol from the glass concentric nebulizer operated with a gas flow of 0.5 L min^{-1} and the same liquid flow rate as the DIN. Figure 2b is the mass distribution for an aerosol produced from from a glass concentric nebulizer operated under the usual conditions of 1 ml min^{-1} liquid flow rate and 0.75 L min^{-1} gas flow rate after it had been passed through a spray chamber.

When the DIN was used for ICP-MS, the maximum signal was observed for a nebulizer gas flow rate of 0.5 L min^{-1}. However, Figure 1a shows that even when the DIN was operated at a nebulizer flow of only 0.2 L min^{-1}, few large droplets were detected. In fact, at this low nebulizer gas flow only 119 droplets had a diameter larger than 20 μm out of over 370,000 detected. As the nebulizer gas flow increased (Figure 1b, 1c), the larger drops were lost and the amount of aerosol contained in particles with diameters from 6 to 10 μm increased. For

usual DIN operating conditions (Figure 1c), 99.9 % of the aerosol mass was contained in particles less than 20 μm in diameter.

It is interesting that the fraction of aerosol contained in particles less than 6 μm diameter changed only slightly with nebulizer gas flow rate for the DIN. For example, the fraction of aerosol contained in droplets with diameters between 2 μm and 4 μm was about 5 % for each gas flow rate. Thus, the net effect of a higher nebulizer gas flow rate was the elimination of the largest particles to produce a narrower particle size distribution.

Figure 2a shows the aerosol distribution for a glass concentric nebulizer (Meinhard C) operated with a sample flow rate 10 times lower than usual. Theoretically, "starving" a pneumatic nebulizer by operating it at a reduced liquid flow rate should produce a finer aerosol (13-16). Still, the aerosol from the conventional nebulizer had a much wider size distribution than that from the DIN. In fact, about 5 % of the aerosol from the conventional nebulizer was contained in droplets larger than 70 μm. This demonstrated that the reduction in aerosol size was not simply due to the low liquid flow rate typically used with the DIN.

Table I compares the Sauter mean diameter (D_{32}), the standard deviation of the aerosol mass distribution, and the 90 % mass diameter for the DIN and the Meinhard nebulizer. The first four rows of data were from measurements directly on the aerosol produced by the nebulizers. The last row of data was measured from the aerosol produced by a Meinhard nebulizer after it passed through a Scott-type

dual-pass spray chamber. In the latter case, a liquid flow rate of 1000 μL min^{-1} was used to mimic the usual analytical practice.

The Sauter mean diameter described the ratio of the aerosol volume to surface area. A small value indicated a fine aerosol. No definite trend in the Sauter mean diameter was found when the DIN was operated at different argon flow rates. However, there was a difference between the Sauter mean diameter for the DIN aerosol and the aerosols produced by the glass concentric nebulizer. The aerosol from the starved Meinhard nebulizer had a Sauter mean diameter 5 μm larger than that of the DIN aerosol. This was consistent with the data in Figures 1c and 2a. When the Meinhard nebulizer was used with a spray chamber, the resultant aerosol had a Sauter mean diameter 3 μm smaller than that produced by the DIN. The value determined (4.1 μm) was similar to the value measured previously by Canals et al. for a similar aerosol when using an instrument based on Fraunhofer scattering (17). A spray chamber can be used to produce a finer aerosol than the DIN, but it was at the cost of poor sample transport efficiency, increased memory effects for important elements such as Hg and B, and poorer precision (5,7).

The standard deviation of the aerosol mass distribution decreased two-fold as the DIN aerosol gas flow rate increased from 0.2 to 0.5 L min^{-1}. As stated above, this was due primarily to the production of fewer large droplets. For the aerosol leaving the spray chamber the standard deviation was slightly smaller than that produced by the DIN. However, the standard deviation for the aerosol directly from the

glass concentric nebulizer was larger than the Sauter mean diameter. This is indicative of a distribution skewed toward large droplets.

The aerosol droplet diameter which represented the 90 % point on a cumulative mass distribution curve was called the 90 % mass diameter. This parameter decreased as the DIN nebulizer gas flow rate increased. For normal DIN operating conditions, more than 90 % of the aerosol mass was contained in particles less than about 12 μm in diameter. In contrast, the glass concentric nebulizer produced an aerosol with a 90 % cut-off diameter of over 36 μm. This was further evidence that the DIN produced a finer aerosol.

Both the DIN and the Meinhard nebulizer are concentric nebulizers which had the same size (~ 15 μm) annular gap for the nebulizer gas flow. Yet when they were operated with the same aerosol gas and sample flow rates, the two aerosols had different size distributions. One explanation for this is that the amount of interaction between the nebulizer gas and the sample liquid may have been different for the two nebulizers. Sample-gas interaction has been identified as an important factor in aerosol production (13). The main differences between the two nebulizers that could have affected the sample-gas interaction were that the glass concentric nebulizer sample delivery capillary had a larger i.d. (300 μm vs. 40 μm) and a thicker wall (90 μm vs. 52 μm) than the fused silica capillary used with the DIN. It is possible that use of narrower capillary dimensions for the DIN promoted closer contact between the nebulizer gas and the sample as it emerged from the sample delivery tube. In addition, because the

sample capillary was larger, the area of the 15 μm annular gap between the concentric tubes was 3 times larger for the glass concentric nebulizer. Thus, for the same gas flow rate, the nebulizer gas velocity was 3 times lower for the glass concentric nebulizer than for the DIN. The higher gas velocity with the DIN should also reduce the aerosol droplet size.

Conclusion

The DIN produced an aerosol superior to that from a glass concentric nebulizer operated under the same conditions. The DIN aerosol was only slightly larger than the aerosol from the glass concentric nebulizer after passage through a spray chamber. The measurements presented here support previous statements concerning the absence of large droplets in the aerosol produced by the DIN. Furthermore, the data indicate that it is possible to construct an ICP nebulizer which does not produce significant numbers of droplets with diameters greater than 16 μm (Figure 1c). Thus the elimination of the spray chamber, which until now has been a major impediment in the sample introduction process for ICP spectroscopy, may be possible without sacrificing precision or detection limits (5).

Literature Cited

1. Lawrence, K. E.; Rice, G. W.; Fassel, V. A. Anal. Chem. 1984, 56, 289-292.
2. LaFreniere, K. E.; Rice, G. W.; Fassel, V. A. Spectrochim. Acta, Part B 1985, 40B, 1495-1504.
3. LaFreniere, K. E.; Fassel, V. A.; Eckels, D. E. Anal. Chem. 1987, 59, 879-887.
4. Avery, T. W.; Chakrabarty, C.; Thompson, J. J. Appl. Spectrosc. 1990, 44, 1690-1698.
5. Wiederin, D. R.; Smith, F. G.; Houk, R. S. Anal. Chem. 1991, 63, 219-225.
6. Wiederin, D. R.; Smyczek, R. E.; Houk, R. S. submitted for publication in Anal. Chem.
7. Smith, F. G.; Wiederin, D. R.; Houk, R. S.; Egan, C. B.; Serfass, R. E. submitted for publication in Anal. Chim. Acta.
8. Olsen, S. D.; Strasheim, A. Spectrochim. Acta, Part B 1983, 38B, 973-975.
9. Hodkinson, J. R. Appl. Optics 1966, 5, 839-844.
10. Dave, J. V. Appl. Optics 1971, 10, 2035-2044.
11. Baumgardner, D.; Cooper, W. A.; Dye, J. E. In Liquid Particle Size Measurements Techniques; Hirleman, E. D.; Bachalo, W. D.; Felton, P. G., Eds.; ASTM STP 1083; American Society for Testing and Materials: Philadelphia, 1990, 115-127.

12. Scott, R. H.; Fassel, V. A.; Kniseley, R. N.; Nixon, D. E. Anal. Chem. 1974, 46, 75-80.

13. Sharp, B. L. J. Anal. Atom. Spectrom. 1988, 3, 613-652.

14. Browner, R. F.; Boorn, A. W.; Smith, D. D. Anal. Chem. 1982, 54, 1411-1419.

15. Browner, R. F.; Boorn, A. W. Anal. Chem. 1984, 56, 786A-798A.

16. Canals, A.; Hernandis, V.; Browner, R. F. J. Anal. Atom. Spectrom. 1990, 5, 61-66.

17. Canals, A.; Hernandis, V.; Browner, R. F. Spectrochim. Acta, Part B 1990, 45B, 591-601.

Table I. Aerosol size measurements for the DIN and Meinhard C nebulizers.

Nebulizer	Sample flow rate ($\mu L\ min^{-1}$)	Gas flow rate ($L\ min^{-1}$)	Sauter mean diameter (μm)	Standard deviation[a] (μm)	90 % mass diameter[b] (μm)
DIN	100	0.2	7.6	4.8	16.0
DIN	100	0.4	7.8	3.0	12.9
DIN[c]	100	0.5	7.1	2.6	11.4
Meinhard C (no spray chamber)	100	0.5	12.0	16.3	36.2
Meinhard C[d] (spray chamber)	1000	0.75	4.1	1.9	6.7

[a]Standard deviation of droplet mass distribution.
[b]90 % point on the cumulative mass distribution curve.
[c]Usual DIN operating conditions.
[d]Usual Meinhard operating conditions.

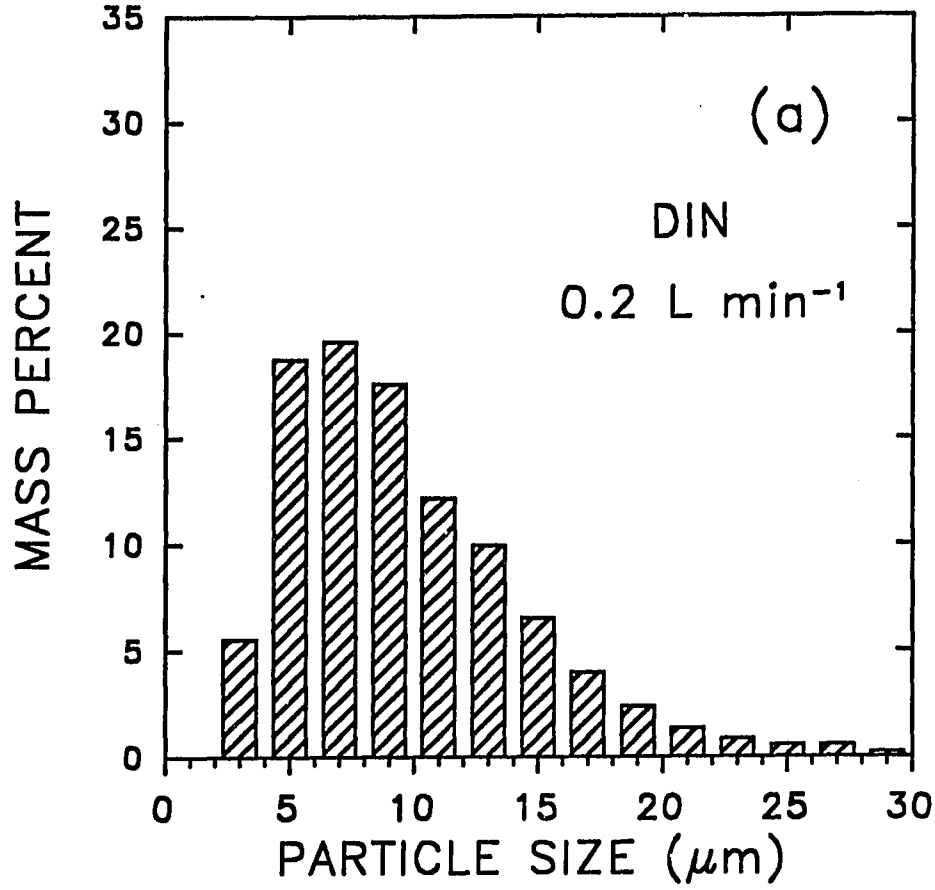

Figure 1. The effect of nebulizer gas flow rate on the DIN aerosol mass distribution when water was nebulized at 100 μL min^{-1}. The gas flow rates were: (a) 0.2, (b) 0.4, and (c) 0.5 L min^{-1}. The distribution for the usual DIN operating conditions is shown in (c).

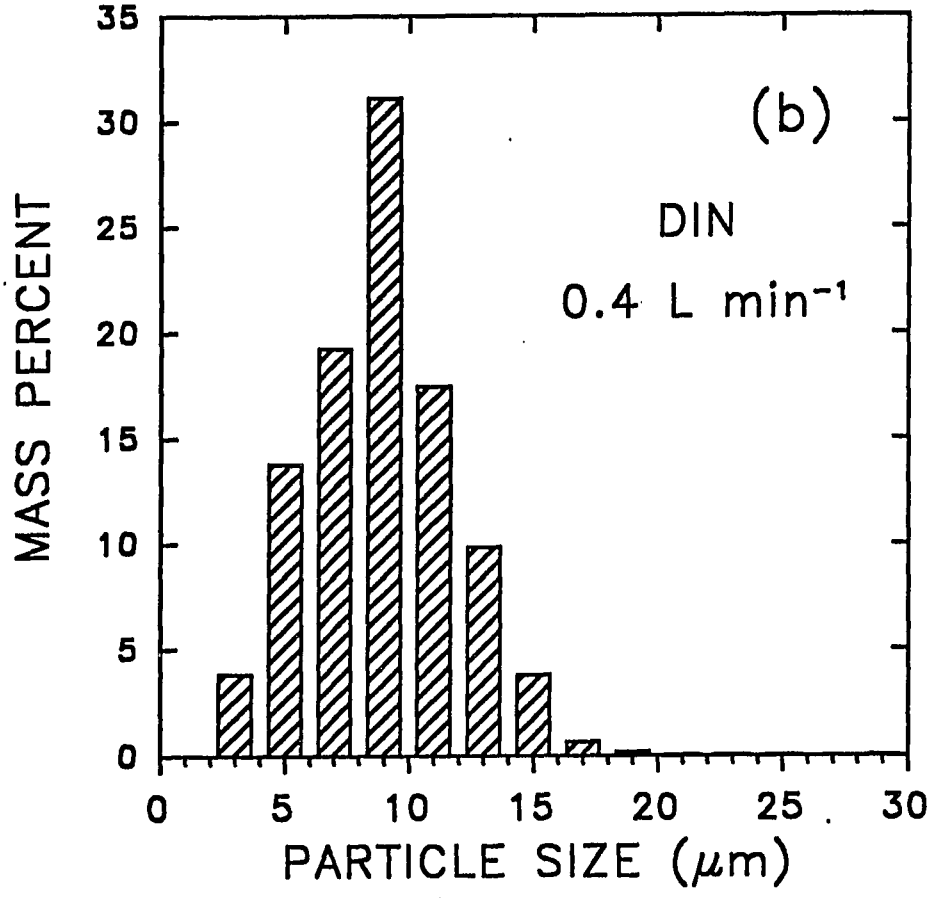

Figure 1. (continued)

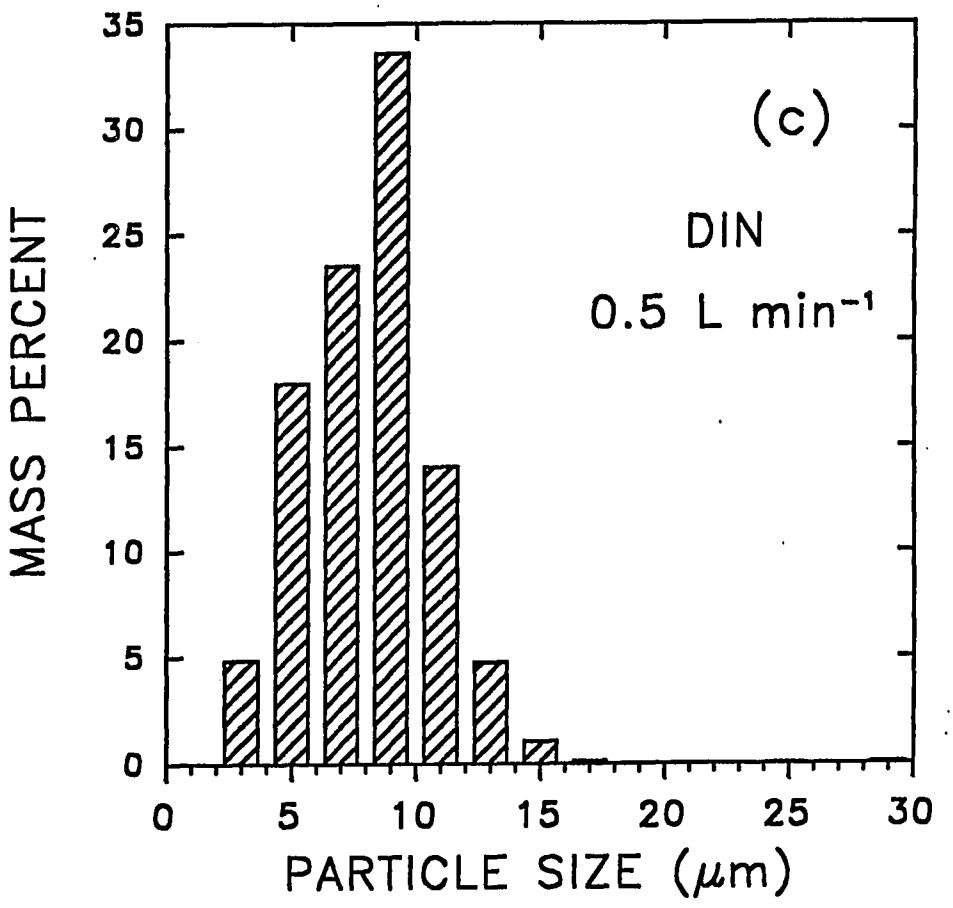

Figure 1. (continued)

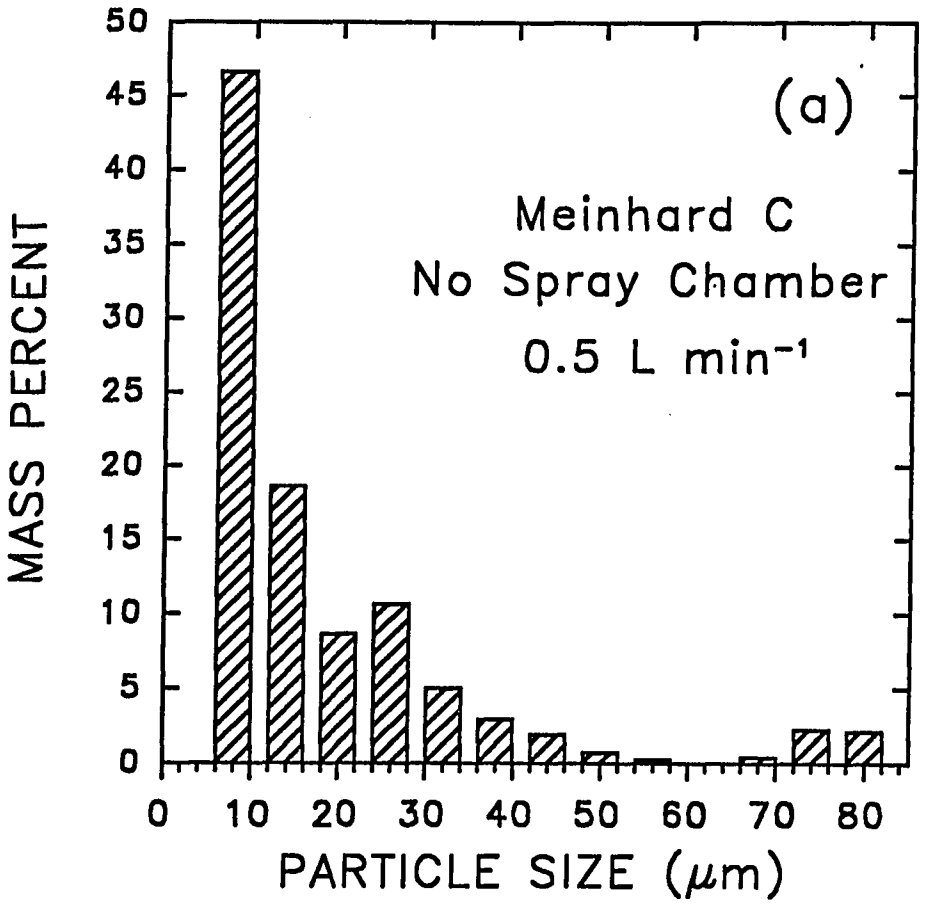

Figure 2. Aerosol mass distribution from a Meinhard C nebulizer when water was nebulized. In (a) the nebulizer liquid flow was 100 μL min^{-1} and the gas flow was 0.5 L min^{-1}. For (b) the liquid flow was 1000 μL min^{-1} and the gas flow was 0.75 L min^{-1}, but the aerosol passed through a Scott-type spray chamber prior to the measurement. Note that the horizontal scale is different in (a) and (b).

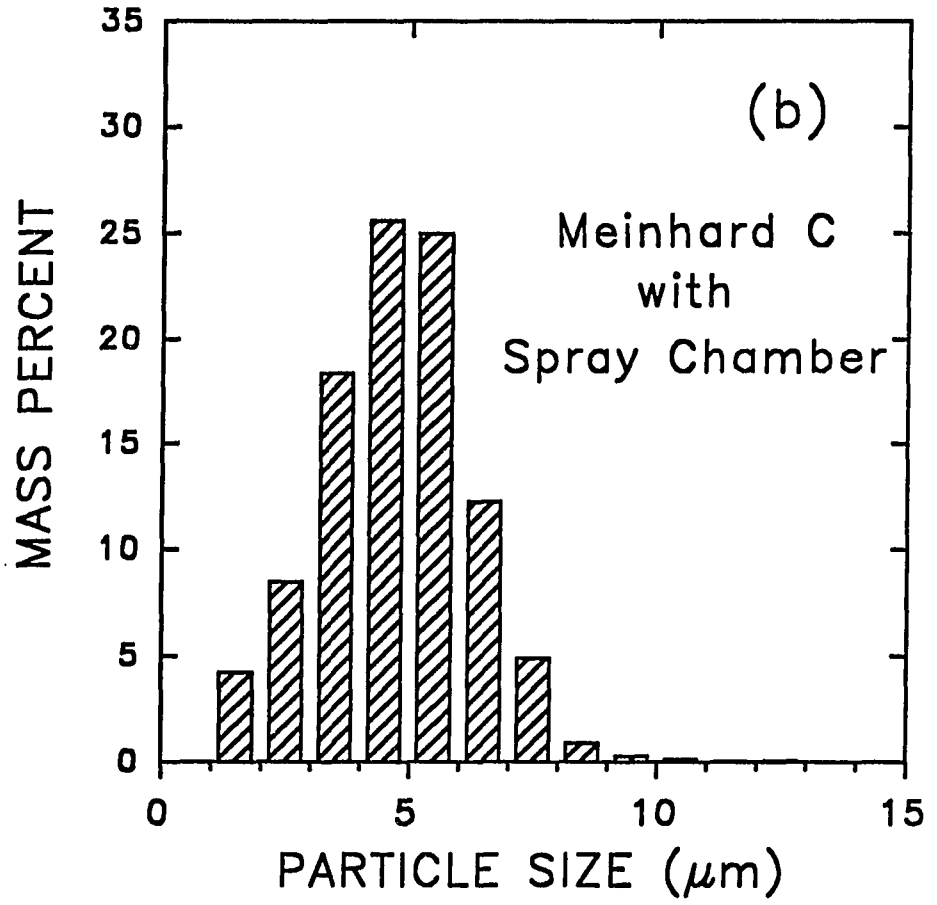

Figure 2. (continued)

SECTION IV.

ON-LINE STANDARD ADDITIONS WITH DIRECT INJECTION NEBULIZATION FOR INDUCTIVELY COUPLED PLASMA MASS SPECTROMETRY

Introduction

Inductively coupled plasma mass spectrometry (ICP-MS) is an excellent technique for trace elemental analysis in solutions containing low levels of dissolved solids. However, for solutions with high salt content, such as urine or seawater, quantification is complicated by sample matrix effects (1,2). The sample matrix can change instrument sensitivity, preventing the use of external calibration methods. Techniques used to compensate for matrix effects include isotope dilution (3-6), internal standardization (7-10), and standard additions (11). The relative merits of these techniques are compared in the literature (12-14).

Standard additions is suitable for matrix correction because, in essence, instrument sensitivity is determined for each sample matrix. However, traditional standard additions is bedeviled by time consuming steps, involving manual preparation of numerous sample and standard solutions. Standard additions employing conventional ICP nebulizers also requires either a relatively large sample volume or a large dilution of the sample. Furthermore, the possibility exists for contamination or error during sample manipulation.

Flow injection techniques have been used for ICP analyses to reduce sample consumption and hasten sample analysis for on-line isotope dilution (15). However these experiments were conducted using conventional nebulizers which were limited by broadening of the flow injection profiles and by long nebulizer wash times. We recently described a microconcentric nebulizer for ICP-MS, termed a direct injection nebulizer (DIN), which was positioned inside the torch injector tube (16). The DIN had improved precision (RSD = 0.5%), a low sample consumption rate (0.1 ml min^{-1}), and exhibited rapid sample change-over capabilities, requiring only 3 s for rinse-in and less than 15 s for rinse-out. This paper describes utilization of the DIN for on-line standard additions to provide rapid, multielement determinations that expend only 0.5 ml of sample and require little solution manipulation.

Experimental

Typical instrumental operating conditions are listed in Table I. The flow scheme for on-line standard additions is shown schematically in Figure 1. Carrier solvent from a gas displacement pump (GDP) (16) went through 1.62 mm o.d. x 0.5 mm i.d. tefzel tubing (A, Figure 1) to a 0.25 mm i.d. PEEK tee (B, Figure 1). The tee was connected to each of two high-pressure metal-free flow injection valves (C, D, Figure 1) using 1.62 mm o.d. x 0.5 mm i.d. tefzel tubing (E, Figure 1). Transfer lines made from 50 μm i.d. fused silica capillary tubing (F,

Figure 1) connected the exit port of each flow injection valve to a second 0.25 mm i.d. PEEK tee (G, Figure 1). To facilitate connection of the fused silica to the valves and tee, a section of PEEK tubing (1.62 mm o.d. x 0.250 mm i.d. x 4 cm long) was glued with epoxy to each end of the fused silica transfer lines. The fused silica was then attached to the valves and tee by slipping standard 1/16" (1.62 mm) fittings over the PEEK sleeves. Another length of fused silica tubing (H, Figure 1, 50 μm i.d. x 200 μm o.d.) delivered the liquid stream from the PEEK mixing tee to the DIN nebulizer tip. The total volume between the valves and the ICP was ~ 3 μL.

Operating procedures

Ordinary flow injection techniques were employed. When either flow injection valve was in the LOAD position 2 % nitric acid flowed from the valve, through the mixing tee, and into the DIN. When the valves were in the INJECT position, the carrier solvent passed through a loop on the valve, pushing its contents into the mixing tee. The sample introduction valve (C, Figure 1) was fitted with a large loop (250 μL or 500 μL), while the standards valve (D, Figure 1) had a smaller loop (40 μL or 50 μL). The pressure on the gas displacement pump was adjusted so that the liquid flow reaching the nebulizer was about 100 μL min^{-1}. Since the flow into the DIN was divided between the two valves, the flow rate through either valve was less than 100 μL min^{-1}. When the capillaries connecting each valve to the tee were the same length, the flow rate through each valve was approximately

equal (i.e., ~ 50 μL min^{-1}). Thus a single sample injection provided steady-state signal for 5 to 10 minutes, while the signals from the standard solutions each lasted roughly 1 minute.

DIN modifications

Solids deposited gradually on the tip of the DIN when highly concentrated solutions (> 1%) were nebulized for extended periods. This accumulated solid did not completely plug the nebulizer, instead it deflected the nebulized aerosol and skewed the plasma central channel off-axis. As a result, analyte signal was reduced.

To minimize salt deposition several changes were made to the normal DIN configuration and operating conditions (16). The make-up gas flow was increased from 0.20 L min^{-1} to 0.40 L min^{-1} and the diameter of the injector tube was reduced from 1.75 mm to 1.0 mm. With this configuration the make-up gas flow sheathed the stainless steel nebulizer tip and swept the nebulized aerosol down the axial channel, preventing deposition of solids on the nebulizer tip. To accommodate the 1.0 mm torch injector tube, the o.d. of the stainless steel nebulizer tip was reduced from 1.6 mm to 0.5 mm so the tip could protrude through the injector tube orifice. Accordingly, a thinner alumina tube (1.62 mm o.d. x 0.8 mm i.d.) supported the narrower nebulizer tip. Up to 20% of the analyte signal was lost due to the higher make-up gas flow rate, but such losses were deemed tolerable in exchange for long-term signal stability. Although the outer DIN dimension was reduced, the critical dimensions for aerosol production

(i.e., the inside and outside diameter of the fused silica capillary and the inside diameter of the steel nebulizer) remained unchanged from the previous work (16).

Salt deposition was also reduced by extending the fused silica sample delivery capillary 0.5 mm past the end of the metal nebulizer tip, compared with the 0.1 mm protrusion used previously. At the new capillary position the mist was not noticeably altered, and the analyte signal was comparable to that obtained previously. The fact that the analyte signal did not depend crucially on the exact positioning of the sample capillary within the nebulizer tip showed that assembly of the DIN was not particularly difficult.

Standard additions on freeze-dried urine

A nine element standard additions analysis was performed on reconstituted NIST SRM 2670, toxic metals in freeze-dried urine. To achieve compromise operating conditions over the whole mass range, the instrument was optimized to give maximum signal for ^{114}Cd. The data were acquired in the multielement mode by peak hopping over ten m/z positions using a 0.5 s measurement time, a 20 ms dwell time, and 1 measurement per peak. The most abundant isotope for each of the nine elements in Table II was monitored except for ^{60}Ni and ^{65}Cu, which were used to avoid several interferences at ^{58}Ni and ^{63}Cu (2, 3, 17). Also, m/z = 118 was monitored to correct for the Sn contribution to the ^{114}Cd signal. The instrument software plotted the signal from only 4 masses during the experiment. After data acquisition, all the

count rate measurements were dumped to the printer and were analyzed further with a spread sheet program.

To correct for background, the count rate while nebulizing 2% nitric acid was subtracted from the analyte signal. The background count rate was generally less than 1% of the analyte count rate when the sample was nebulized. However, since the $^{202}Hg^{+}$ count rates were typically only 400 to 500 counts s^{-1} (due to the high ionization energy for Hg and the ~ 30 % abundance at m/z = 202) the background for Hg was about 8 % of the total count rate.

The analyte concentration was determined to be the x-axis intercept of a least-squares linear regression plot of the standard concentration versus net signal.

Viscosity studies

Because the gas displacement pump was operated at a constant back pressure, solution viscosity affected the flow rate. To investigate viscosity effects, a series of solutions having viscosities (η) relative to that of water (η_o) of η/η_o = 1.000, 1.008, 1.018, 1.072, 1.123, 1.274, 1.421, 1.658, 2.043, and 5.016 were prepared by mixing the appropriate proportions of ethylene glycol and water (18). Each solution was spiked with Tl to a concentration of 0.5 mg L^{-1}. Since the viscosity of the standard solutions can be controlled, only the effects of sample solution viscosity were important. The effect of viscosity on sample flow rate and the corresponding effects on the flow injection peak height, width, and area were studied.

The instrument was optimized to give maximum signal for Tl when nebulizing a solution with $\eta/\eta_o = .1.00$. Solutions containing Tl were introduced through the sample loop; a 0.5 mg L^{-1} Pb solution in deionized, distilled water was introduced through the standard loop. The signals from $^{205}Tl^+$ and $^{208}Pb^+$ indicated passage of the respective solutions through the nebulizer. The instrument was operated using a 0.4 s measurement time, a 20 ms dwell time, and 1 measurment per peak so that one data set was collected each second. The liquid flow rate was estimated from the loop volume divided by the full width at half maximum of the resulting flow injection peak. The peak height was the mean of the steady-state signal obtained for the flow injection peak. The peak area was the area under the peak for all points where the signal intensity was greater than 10% of the steady-state signal.

Background studies

The effect of a concentrated salt matrix on the background was investigated by preparing solutions containing varying fractions of a reference coastal seawater, CASS-1 (National Research Council Canada). The reference seawater was diluted using distilled deionized water.

Solution preparation

A 1000 ppm Be standard was prepared by dissolving $BeCl_2$ in 2% nitric acid. All other standard solutions were prepared by dilution from 1000 ppm standards (Fisher) using 2% nitric acid (Ultrex II, ultrapure reagent grade, J. T. Baker) in distilled, deionized water

(18 MΩ, Barnstead). For the multielement determination of toxic metals in urine a solution containing 100 ppb Be; 200 ppb Cd; 400 ppb each Pt, Hg, and Pb; and 1 ppm each Mn, Ni, Cu, and Se was prepared in 2% nitric acid. This solution served as the most concentrated standard. Aliquots of this solution were diluted 2x and 4x using 2% nitric acid to provide the other standards for analysis of urine. The standard solutions were prepared in the same solvent (usually 2 % nitric acid) that was used to fill the GDP reservoir so that the matrix did not change when the standard was introduced. NIST SRM 2670 (toxic metals in freeze-dried urine) was reconstituted as instructed and nebulized without further dilution.

Results and Discussion

DIN procedures

The low dead volume of the DIN makes it particularly well-suited for on-line standard additions with inductively coupled plasma spectroscopy because solutions rapidly rinse-in and memory effects are minimal. Thus measurements may be made quickly on a steady-state signal while consuming only a small volume of sample.

Figure 2 shows typical profiles for the on-line standard additions procedure. The mass spectrometer hopped over four m/z positions to collect the data for Be, Se, Hg, and Tl. Initially (time = 0) 2% nitric acid flowed through each injection valve. At 60 seconds a "sample" containing 10 ppb each Be, Se, Hg, and Tl in 2% nitric acid

was injected through the 500 μL loop on the sample valve. Meanwhile, 2% nitric acid continued to flow through the standard valve. Analyte in the sample produced a long, flat signal pulse. Three multielement standard solutions were then sequentially injected via the standard valve. At 145 seconds the first standard, a 50 μL solution containing 10 ppb of each element in 2% nitric acid, was introduced. From 145 seconds to 200 seconds the signals observed were due to the analyte in the sample plus the standard. At 200 seconds the standard valve was switched to the LOAD position so that 2% nitric acid once more flowed through the standard valve. The standard solution rinsed out, and the signal was once again due only to analyte in the sample. The 20 ppb and 30 ppb standard solutions were subsequently introduced in the same manner. After the standard additions was completed (time = 475 seconds), the sample was rinsed out by switching the sample valve to the LOAD position. The remaining sample in the loop was then manually rinsed in preparation for the next sample.

Another attractive aspect of the on-line standard additions procedure is illustrated in Figure 2. Ideally, the concentrations of the added standards should be comparable to the concentration of the analyte in the sample. For conventional standard additions, a semi-quantitative determination may be required to obtain this information prior to preparation of the standard solutions. With the on-line approach, the analyte concentration can be estimated quickly from the count rate for the sample alone, e.g., at time = 100 s in Figure 2. Appropriate standards can then be readily selected.

Correction for instrumental drift

When solutions containing >1% salt were continuously nebulized for several minutes, a downward drift in analyte count rate of up to 10 % over a 5 minute period was occasionally observed. Presumably this was due to partial plugging of the ICP-MS sampling orifice, or to skewing of the axial channel caused by salt build-up on the nebulizer tip, as described in the Experimental section. Of course, the drift affected the signal from analyte in the standard and sample in the same way.

To correct for drift, the count rate was measured for each m/z before and after the addition of each standard solution. During such time periods the sample solution was mixed with solvent flowing through the standard valve prior to nebulization. Thus this signal was due to the analyte from the sample solution alone. The mean of the count rates before and after the addition of each standard was calculated. This "sample" mean was subsequently used as an internal standard by dividing it into the count rate measured when each standard was added. For example, the signal when the 10 ppb standard was introduced (Figure 2) would be divided by the average of the count rates measured from the flat regions around 100 seconds and 230 seconds. The standard concentration added was then plotted versus the ratio obtained. The abscissa for the point representing the sample solution only (added concentration = 0) was always 1 for this plot. Use of the sample signal as an internal standard allowed correction for instrumental calibration drift between each addition of standard, about once each minute.

Sample and standard flow rates

The flow rates through the sample valve and the standard valve had to be known to calculate analyte concentration because they determined the proportion of standard and sample introduced to the ICP. The flows were determined by measuring the analyte count rate when the same solution was independently introduced through each of the two valves. The ratio of the analyte count rates was proportional to the ratio of the flow rate through the two valves. This count rate method was independently verified by measuring the flow injection peak width when the identical loop was attached to each valve, the peak width being directly proportional to the flow rate. Both methods gave the same flow rate ratio to within 1%.

The relative flow rates through each injection valve could be adjusted by varying the length of the fused silica capillary used to connect the valves to the mixing tee. For instance, when the length of capillary connecting the standard valve to the tee was longer than the one connecting the sample valve to the tee, the liquid flow rate through the standard valve was lower than that through the sample valve. Thus the sample dilution factor was smaller.

Figure 3 shows data used to determine the relative flow rate through the two flow injection valves. The nebulizer and standard additions apparatus were the same as those used when the data presented in Table II were collected. The multielement solution described in the Experimental section was first injected through the standard valve and sample valve independently, then through both

valves simultaneously. The steady-state Be signal from the 40 μL loop on the standard valve (e.g., at time = 50 s) and the steady-state signal measured from the solution in the sample valve (e.g., at time = 125 s) were proportional to the liquid flow rate through each valve. When 100 ppb Be was injected through both loops simultaneously (e.g., at time = 150 s) the total ^{9}Be signal observed was within 1% of the sum of the signals obtained when the two loops were injected independently. For Be (Figure 3) the ratio of the flow through the standard valve to the flow through the sample valve was 0.681. The mean flow ratio for the elements listed in Table II was 0.688 ± 0.008. The standard deviation was within the error of the measurement.

Calculations

The primary difference in calculating analyte concentrations when using off-line compared to on-line standard additions was that the parameters indicating the proportion of standard and sample were not static (volume) but dynamic (flow rate). Equation (1) shows a conventional standard additions equation which has been modified for on-line standard additions by replacing the volume parameters by the relative flow rate parameter, R. For situations where the sample solution and the standard solution had different viscosities (see subsequent discussion), an additional factor, η_x/η_s, was required to describe the relative flow rates through the two loops. For sample solutions containing < 1 % dissolved solids $\eta_x \simeq \eta_s$. In addition, the

nebulizer can be constructed so that R $\simeq$ 1. Equation 1 then reduces to equation 2.

$$S_{X+S} = (m)(C_X + RC_S\eta_X/\eta_S)/(1 + R\eta_X/\eta_S) \quad (1)$$

$$S_{X+S} = 0.5(m)(C_X + C_S) \quad (2)$$

Where:

S_{X+S} = signal from sample plus standard

C_X = unknown analyte concentration in sample

C_S = analyte concentration in standard

m = instrument sensitivity (counts s^{-1} per unit concentration)

R = ratio of standard flow rate to sample flow rate

η_X/η_S = ratio of sample viscosity to standard viscosity

For the standard additions data collected for freeze-dried urine, R = 0.688 because the standard solution passed through a longer length of fused silica, causing it to flow more slowly than the sample solution. The quantity $RC_S\eta_X/\eta_S$ was termed the effective standard concentration, because it corrected the concentration of the standard as injected for flow rate and viscosity effects.

When the least squares line was fit to the data, a plot was made of the effective standard concentration versus analyte count rate. The x axis intercept of a least squares fit to the data gave the concentration of analyte in the sample. Typically the correlation

coefficient of the least squares fit ranged between 0.999 to 0.9999, with the poorer values coming from the elements with low count rates.

Analysis of freeze-dried urine

Table II shows the concentrations found in reconstituted freeze-dried urine (NIST SRM 2670) containing elevated levels of toxic metals. Standard solutions were prepared as described above. Three standards were added in sequence to each of the three urine injections to yield profiles much like those shown in Figure 2. The first column in Table II shows the range of concentrations found for each element over the three determinations. The mean values for the three determinations are listed in the second column. The third column shows the certified or suggested concentrations. The mean concentration found for Ni is about 23 % higher than expected, the other values are within 8 % of the certified or suggested values.

The determined and accepted concentrations in Table II agreed closely even though the urine matrix greatly affected the analyte sensitivity (i.e., the ion count rate per unit concentration). For most elements, sensitivity in the urine matrix was less than that for a 2 % HNO_3 standard by a factor of 5 to 10. For Se, the suppression factor was 30. Thus, this standard additions procedure did correct effectively for a substantial matrix effect.

A possible reason for the high value for the Ni concentration is a spectral interference arising at m/z = 60 due mainly to the molecular ion $^{44}Ca^{16}O^{+}$ (3, 17). Since the interference originates from the Ca

in the sample solution, subtracting the nitric acid blank from the signal cannot correct for it. The inability to correct for spectral interferences originating from components in the sample solution is a weakness of simple standard additions.

Viscosity effects

Because a constant gas pressure was applied to the GDP solvent reservoir, sample viscosity affected sample flow rate. The effect of sample viscosity was studied by injecting mixtures of water-ethylene glycol as described above. Figure 4 shows the effect of viscosity on the width (FWHM) of the flow injection peak for a 20 μL injection. The relationship is fairly linear up to at least a relative viscosity of 5, which corresponds to a solution that is 60 % by weight ethylene glycol. Thus, by simply measuring the sample injection FWHM, the sample viscosity (η_x) may be determined. The ratio η_x/η_s, where η_s is the standard solution viscosity, corrects the flow rate ratio for viscosity effects.

For most solutions which are routinely analyzed by ICP-MS, viscosity effects are minimal. In general, the solution viscosity will change by only 1 % or less when the salt content of the solution is less than 1 % (18). In such situations correction for viscosity effects may not be necessary.

Table III lists the peak heights and areas as a function of the relative viscosity of the sample solution. The viscosity listed is that of the sample solution before it was diluted by the flowing

stream from the standard loop. Solution viscosity affected peak area less than peak height. For solutions having a viscosity up to the equivalent of a 4 % NaCl solution (η/η_o = 1.072), no measurable change in peak area was observed. For solutions with viscosities up to η/η_o = 5, only a 20 % change in peak area was observed.

The reasons for the increase in peak area at high viscosity are uncertain. One possible explanation is as follows. As the viscosity increased, the liquid flow rate decreased. Although these two factors tend to have opposite effects on droplet size, the net effect will be to generate smaller droplets (19). The smaller droplets were then be more completely dissociated, atomized, and ionized within a single region of the plasma, allowing them to be sampled more efficiently.

Background effects

A curious effect was observed when solutions containing several percent salt were nebulized. Figure 5 shows the count rates measured at three m/z positions when solutions containing various fractions of seawater were nebulized with the DIN. When distilled water was nebulized (fraction = 0), the background at each m/z was less than 20 counts s^{-1}. As the proportion of seawater increased, the background count rate increased for m/z = 111 and 209, but at m/z = 9 the background remained constant. Scans over the mass range revealed that the shift in background was not due to contamination because the whole background had been shifted to higher values, across the upper end of the mass range. The scans also showed that the increase in background

began somewhere between m/z = 12 and m/z = 45, the exact position being hard to locate because the count rate was at least 100 counts s^{-1} over that range. Similar increases in background are likely when other highly concentrated matrices are introduced.

Although no explanation for these observations is apparent, the background effect must be considered when performing standard additions with low analyte count rates to prevent a positive error. The magnitude of error will depend upon the true analyte count rate. The change in background is particularly important when peak hopping. We suggest that the background be monitored by hopping to a m/z position devoid of ions (e.g., m/z = 229.5) during data acquisition and using the background measured there to correct for the change in background under the analyte peaks.

Conclusion

Flow injection coupled with the DIN to perform on-line standard additions allows rapid multielement quantification in difficult matrices such as urine. Further extension of the technique for elemental analysis in organic solvents and samples with varying acid concentration should also be possible. Although sample volumes as large as 0.5 ml were used in this study, sample volumes smaller than 100 μL could be analyzed if a single standard injection is used rather than three standards. In addition, the ready capability to determine

the solution flow rate (and vicosity) for each sample allows for corrections to be made for changes in solution viscosity.

Future applications beyond standard additions may include on-line isotope dilution, similar to the method demonstrated by Vicián et. al. (15), except that a DIN would be used in place of a conventional pneumatic nebulizer. In this circumstance an isotopically enriched spike would be introduced through the standard valve to produce a change in the isotopic ratio related to the concentration of the element in the sample and spike. Because flow injection methods are highly amenable to automation, further reduction in manual sample manipulation may be achieved, making on-line standard additions even more attractive.

Literature Cited

1. Olivares, J. A.; Houk, R. S. Anal. Chem. 1986, 58, 20-25.
2. Tan, S. H.; Horlick, G. J. Anal. Atom. Spectrom. 1987, 2, 745-763.
3. Garbarino, J. R.; Taylor, H. E. Anal. Chem. 1987, 59, 1568-1575.
4. McLaren, J. W.; Beauchemin, D.; Berman, S. S. Spectrochim. Acta. Part B 1988, 43B, 413-420.
5. McLaren, J. W.; Beauchemin, D.; Berman, S. S. Anal. Chem. 1987, 59, 610-613.
6. van Heuzen, A. A.; Hoekstra, T.; van Wingerden, B. J. Anal. Atom. Spectrom. 1989, 4, 483-489.
7. Thompson, J. J.; Houk, R. S. Appl. Spectrosc. 1987, 41, 801-806.
8. Lyon, T. D. B.; Fell, G. S.; Hutton, R. C.; Eaton, A. N. J. Anal. Atom. Spectrom. 1988, 3, 265-271.
9. Vanhoe, H.; Vandecasteele, C.; Versieck, J.; Dams, R. Anal. Chem. 1989, 61, 1851-1857.
10. Mulligan, K. J.; Davidson, T. M.; Caruso, J. A. J. Anal. Atom. Spectrom. 1990, 5, 301-306.
11. McLaren, J. W.; Beauchemin, D.; Berman, S. S. J. Anal. Atom. Spectrom. 1987, 2, 277-281.
12. Houk, R. S.; Thompson, J. J. Mass Spectrom. Rev. 1988, 7, 425-461.

13. Taylor, H. E. In Applications of Inductively Coupled Plasma Mass Spectrometry; Date, A. R.; Gray, A. L., Eds.; Chapman and Hall: New York, 1989, Chapter 3.

14. Jarvis, K. E. Handbook of Inductively Coupled Plasma Mass Spectrometry; Blackie: London; 1991.

15. Viczián, M.; Lásztity, A.; Wang, X.; Barnes, R. M. J. Anal. Atom. Spectrom. 1990, 5, 125-133.

16. Wiederin, D. R.; Smith, F. G.; Houk, R. S. Anal. Chem. 1991, 63, 219-225.

17. Vaughn, M.-A.; Templeton, D. M. Appl. Spectrosc. 1990, 44, 1685-1689.

18. Wolf, A. V.; Brown, M. G.; Prentiss, P. G. In Handbook of Chemistry and Physics, 66th ed.; CRC Press: Boca Raton, FL, 1986; pp D-219 ff.

19. Browner, R. F. In Inductively Coupled Plasma Emission Spectroscopy-Part 2; Boumans, P. W. J. M., Ed.; Wiley: New York, 1987; p. 279.

Table I. Instrument Conditions and Operating Procedures.

ICP-MS	Sciex Elan Model 250
ICP torch (DIN torch) (16)	"Short"-type torch
	Injector tube orifice = 1.0 mm
Argon flow rates:	
outer	14 L min^{-1}
intermediate	1.5 L min^{-1}
make-up	0.40 L min^{-1}
DIN nebulizer gas (argon):	
pressure	200 psi
flow rate	1.0 L min^{-1}
Plasma forward power	1.50 kW
ICP sampling position	On center, 20 mm above load coil
Gas Displacement Pump (GDP) (16):	
pressure	1200 psi
solvent	2% nitric acid
total liquid flow rate	100 μL min^{-1}, divided into sample and standard flows
Detector voltage:	-4000 V
Ion lens settings:	
Einzel 1 & 3	-19.80 V
plate	-11.00 V
barrel	+5.42 V
photon stop	-4.80 V
Flow injection valves	Rheodyne model # 9010 metal-free
Tee	PEEK 0.250 mm i.d., 1/16" fittings

Table II. Determination of Toxic Metals in Freeze-Dried Urine SRM 2670 (Elevated Level)

Element and m/z	Range of Concentrations Found ($\mu g\ ml^{-1}$)	Mean Concentration Found ($\mu g\ ml^{-1}$) (3 determinations)	Certified (Suggested) Value ($\mu g\ ml^{-1}$)
Be 9	0.030 - 0.034	0.032	(0.033)
Mn 55	0.308 - 0.327	0.32	(0.33)
Ni 60	0.368 - 0.372	0.37	(0.30)
Cu 65	0.366 - 0.394	0.38	0.37 $\pm$ 0.03
Se 82	0.446 - 0.473	0.46	0.46 $\pm$ 0.03
Cd 114	0.083 - 0.090	0.087	0.088 $\pm$ 0.003
Pt 195	0.120 - 0.133	0.13	(0.12)
Hg 202	0.084 - 0.107	0.97	0.105 $\pm$ 0.008
Pb 208	0.104 - 0.106	0.105	0.109 $\pm$ 0.004

Table III. Effect of Relative Viscosity on Peak Height and Area.[a]

Relative Viscosity (η/η_o)	Peak Height (counts s^{-1})	Peak Area (counts)
1.000	4.15×10^5	1.10×10^7
1.008	4.11	1.09
1.018	4.26	1.11
1.072	4.04	1.09
1.123	4.27	1.24
1.274	3.91	1.29
1.421	3.30	1.22
1.65	2.94	1.28
2.043	2.49	1.28
5.016	1.15	1.31

[a]20 μL injection volume. Analyte was 0.5 mg L^{-1} Tl; m/z = 205 monitored.

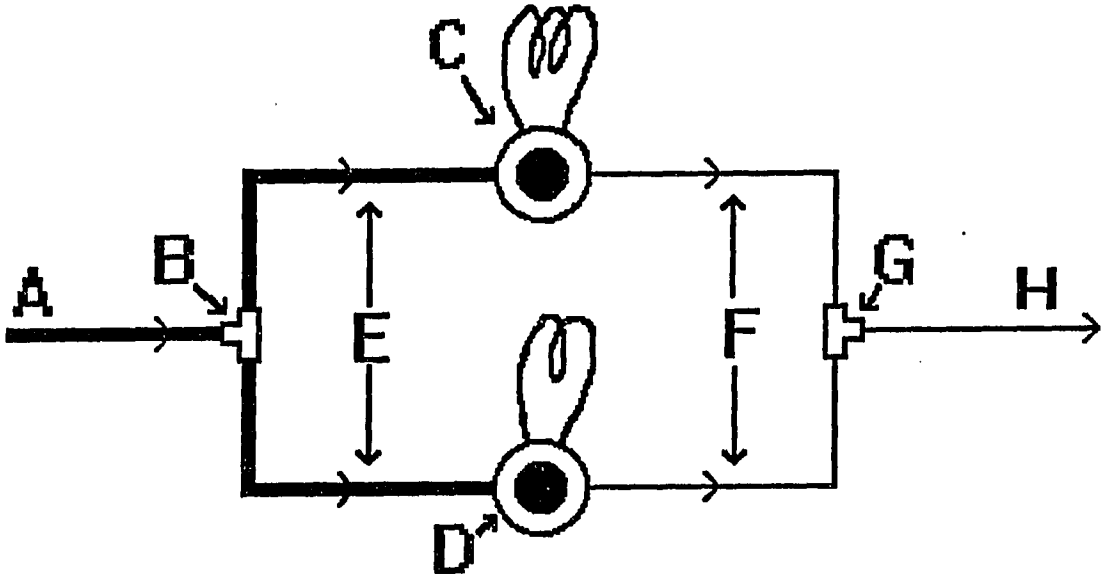

Figure 1. Diagram of standard additions flow scheme: [A] tefzel tubing (0.5 mm i. d.) from gas displacement pump (GDP), [B] PEEK splitter tee, [C] flow injection valve for sample solution, [D] flow injection valve for standard solutions, [E] tefzel tubing, [F] fused silica tubing (50 μm i. d.), [G] PEEK mixing tee, [H] fused silica tubing leading to nebulizer.

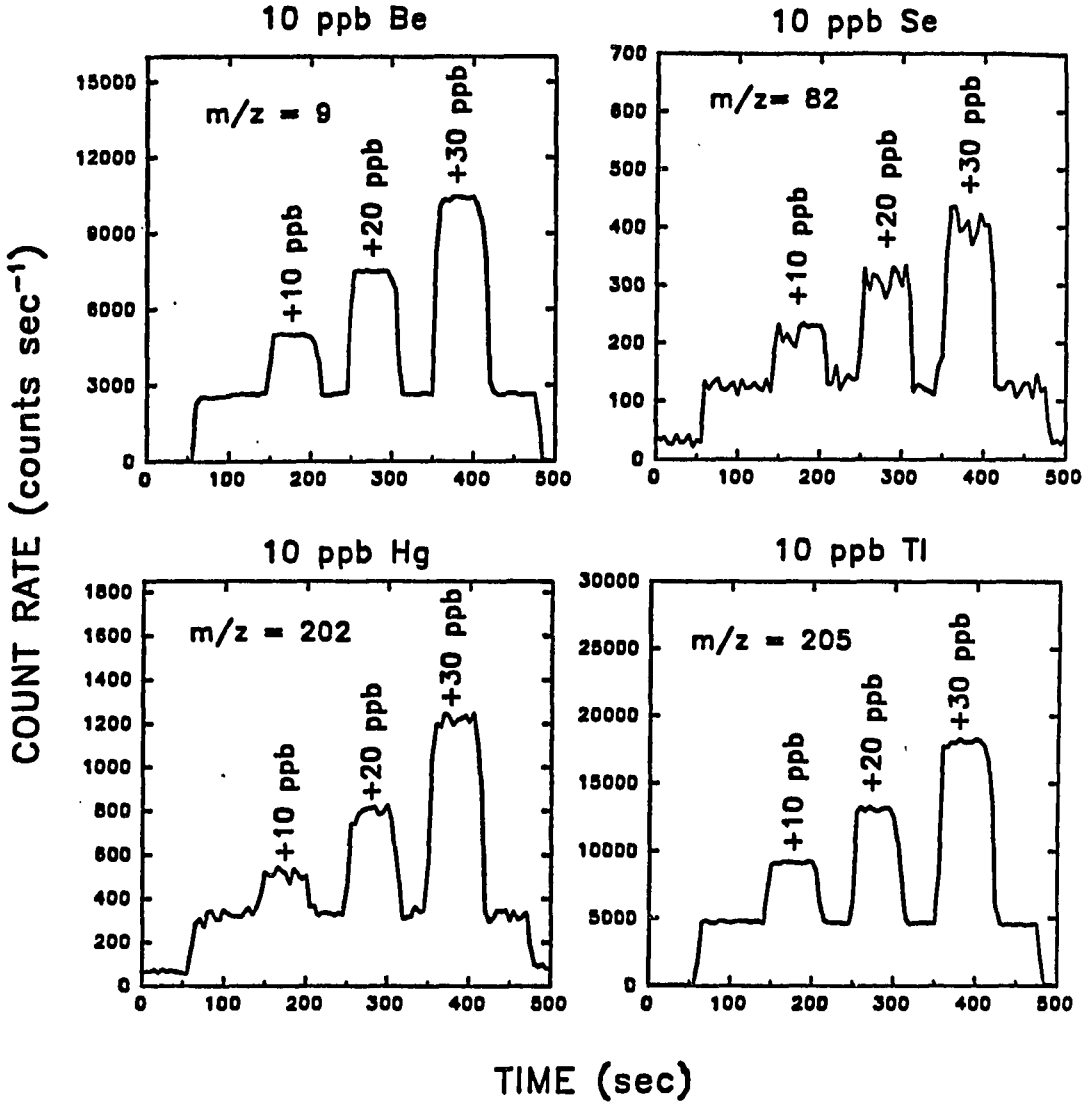

Figure 2. Signals for three standard injections (40 μL) containing 10, 20, and 30 ppb each Be, Se, Hg, and Tl are shown atop the signal from a single 500 μL injection of "sample" containing 10 ppb of each element in 2 % nitric acid.

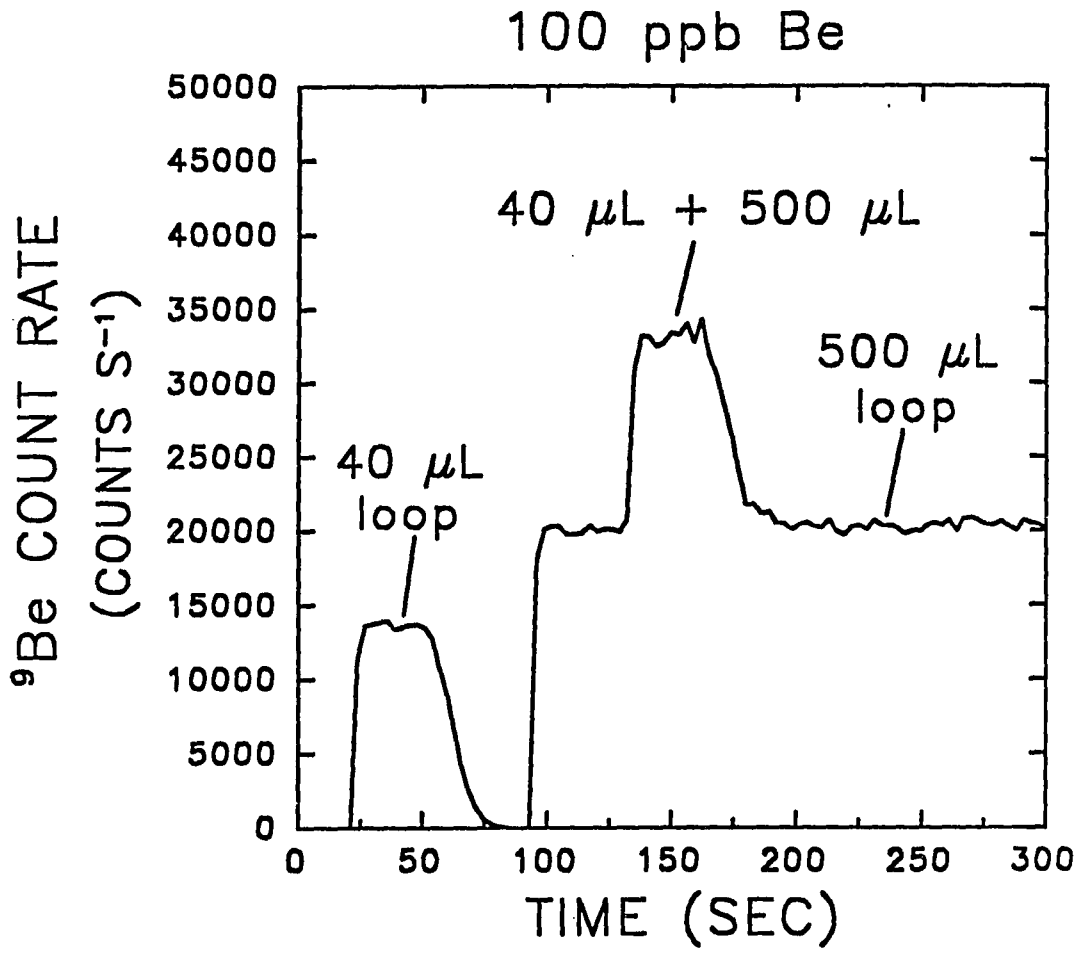

Figure 3. Be signal from the standard loop (40 μL) and sample loop (500 μL) injected independently (left) and simultaneously (right). The liquid flow rate through the standard loop was 0.681 of that through the sample loop.

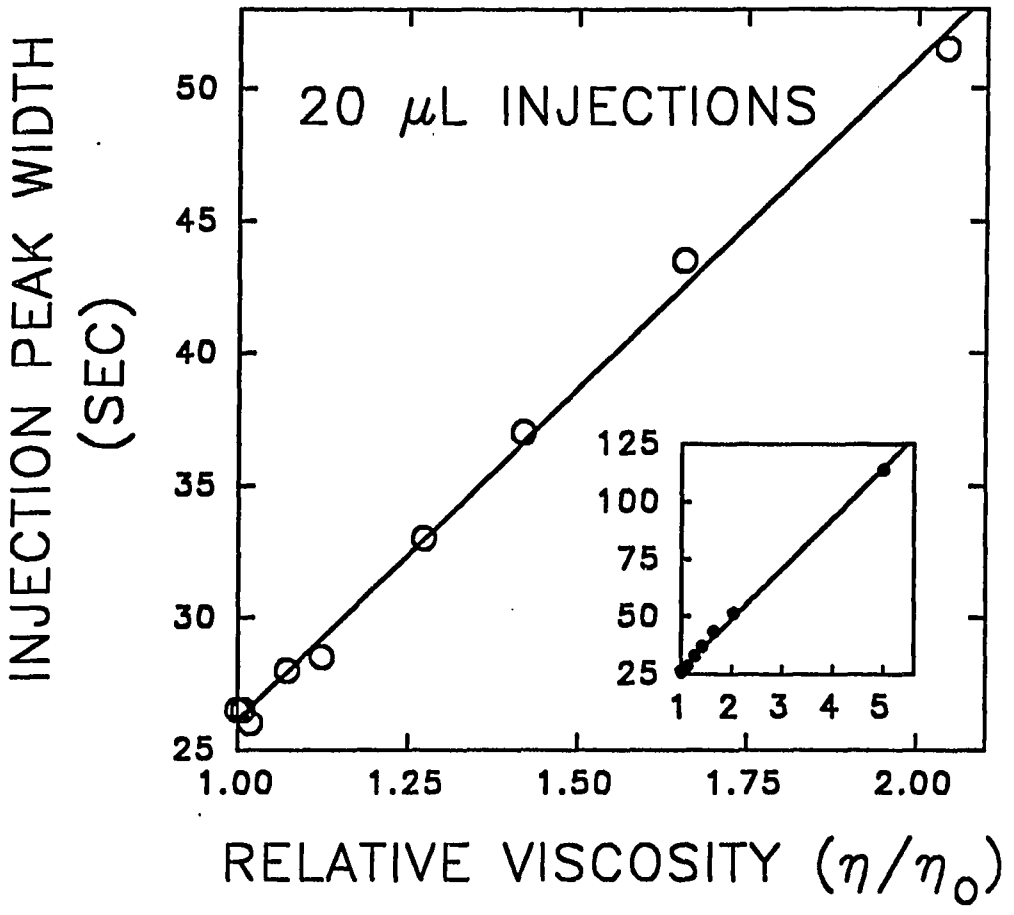

Figure 4. Effect of viscosity on flow injection peak width.

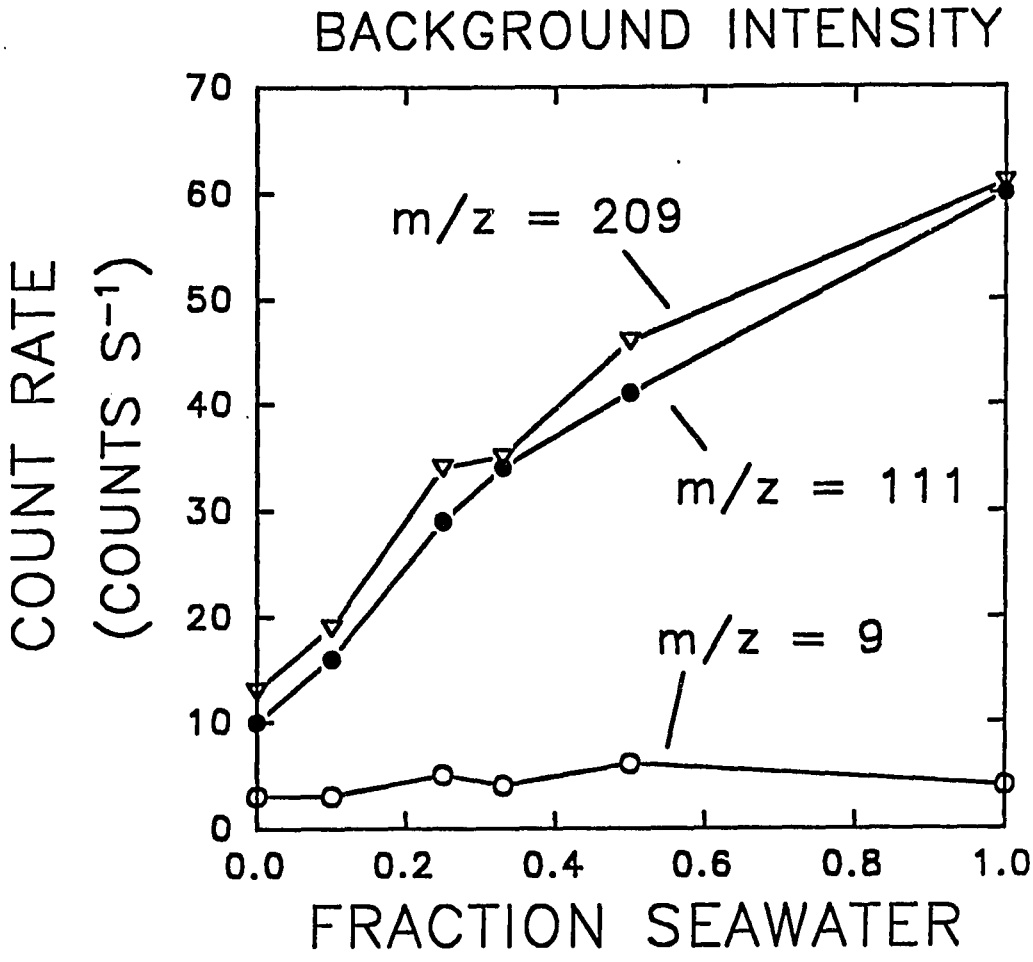

Figure 5. Change in background when seawater is nebulized. Fractional solutions were prepared in distilled, deionized water. Scans across the mass range showed no peaks at m/z = 111 or 209, indicating the change in background was not due to sample contamination.

SUMMARY

This dissertation focuses on three main weaknesses of previous ICP sample introduction techniques. Cryogenic desolvation allows the determination of trace metals in volatile organic solvents. The DIN exhibits high analyte transport efficiency, allowing the determination of a wider range of elements, in smaller samples, at higher precision, more quickly than any previous sample introduction system. On-line standard additions mitigates the vexing problem of elemental quantification by ICP spectrometry where severe sample matrix effects exist.

The capabilities of the DIN and cryogenic desolvation suggest several possible areas for future research. Use of cryogenic desolvation to reduce the amount of solvent which reaches the plasma promises to be even more important for ICP-MS than it is for ICP-AES. This is because solvent-derived polyatomic ion interferences, such as refractory oxides, are the main source of spectral interferences in ICP-MS (64). If the amount of water can be drastically reduced by using cryocondensation, a number of interferences in ICP-MS can be reduced or nearly eliminated. Second, the cryogenic desolvation method may allow currently available chromatographic separation methods to be interfaced to the ICP. Previously, the chromatographic separation was limited because ionization conditions in the ICP deteriorated when organic modifiers, such as methanol and acetonitrile, were added (72). Third, use of cryogenic desolvation

will allow the determination of analytes which have been preconcentrated by extraction into an organic solvent. Currently, an inconvenient back extraction into aqueous solvent is required prior to nebulization (73). Finally, combination of a DIN-type concentric nebulizer with a small spray chamber and cryogenic desolvation might retain most of the advantage of the DIN for quick rinse-out while eliminating solvent derived interferences in the ICP. This system would also be useful for combining liquid chromatography with ICP-MS.

A number of future projects employing the DIN are also envisioned. The first involves further refinement and development of the DIN. The DIN aerosol might be improved by changing the dimensions of the fused silica sample delivery capillary or other geometrical dimensions. Only a few sizes of capillary tubing were investigated during the development of the current DIN. A scientific study of the effect of capillary wall thickness and internal diameter, as well as the width of the annular space for the nebulizer gas, may allow production of an even better aerosol. Such experiments would rely upon both measurements of the aerosol size distribution and empirical measurements of the analyte signal produced in the ICP. A further outgrowth of these experiments may be a better understanding of the processes involved in pneumatic nebulization, an area which has advanced little in the past 50 years (74).

A specific area of investigation is the use of thin-walled (< 20 μm), but larger bore (~ 75 μm) polyimide tubing instead of fused silica for sample delivery. The thin wall may allow better

interaction of the nebulizer gas with the sample liquid, thus improving the mist while the larger bore will reduce the liquid pressure required for DIN operation. In addition, polyimide tubing, unlike fused silica, is resistant to HF, which is often used for dissolving geological samples prior to ICP analysis.

Applications of the DIN include use of its low volume and high transport efficiency for interfacing the ICP with microcolumn liquid chromatography. The low dead volume of the DIN will retain chromatographic resolution and the high transport efficiency should improve detection limits by an order of magnitude or more.

The DIN may also be used to perform on-line functions, using apparatus similar to that used for standard additions. Use of flow injection makes the on-line preconcentration and matrix separation method of Plantz et al. (75) appealing for use with the DIN. In addition, on-line isotope dilution (76) or even standard additions using isotopically enriched standards should be feasible.

No nebulizer combines as many of the desirable characteristics of the ideal nebulizer as the DIN does. For this reason it is tempting to predict that the DIN will become a general purpose nebulizer for ICP spectrometry. The DIN is probably not the "holy grail" of sample introduction, primarily because when it is used in the direct injection mode solvent effects cannot be eliminated by desolvation. In addition, undissolved particulates in some samples may block the nebulizer. Still, the DIN is a significant improvement over other nebulizers and it should become a strong competitor in the near

future. The DIN will improve on the already strong advantage of ICP over flame atomic absorption spectroscopy and the DIN will enable ICP-MS to replace cold vapor atomic absorption for the determination of Hg in environmental samples. For these reasons, the DIN will succeed not only because of its advantages over other nebulizers for ICP spectrometry, but because it will strengthen the position of the ICP relative to other methods used for elemental analysis.

ADDITIONAL LITERATURE CITED

1. Fassel, V. A. Science 1978, 202, 183-191.
2. Fassel, V. A.; Kniseley, R. N. Anal. Chem. 1974, 46, 1110A-1120A, 1155A-1164A.
3. Fassel, V. A. Pure Appl. Chem. 1977, 49, 1533-1545.
4. Fassel, V. A. Anal. Chem. 1979, 51, 1290A-1308A.
5. Houk, R. S.; Fassel, V. A; Flesch, G. D.; Svec, H. J.; Gray, A. L.; Taylor, C. E. Anal. Chem. 1980, 52, 2283-2289.
6. Douglas, D. J.; Houk, R. S. Prog. Anal. Atom. Spectrosc. 1985, 8, 1-18.
7. Houk, R. S. Anal. Chem. 1986, 58, 97A-105A.
8. Houk, R. S.; Thompson, J. J. Mass Spectrom. Revs. 1988, 7, 425-461.
9. Douglas, D. J. In Inductively Coupled Plasmas in Analytical Atomic Spectrometry, 2nd ed.; Montaser, A.; Golightly, D. W., Eds.; VCH Press: New York, in press.
10. Browner, R. F.; Boorn, A. W. Anal. Chem. 1984, 56, 786A-798A.
11. Browner, R. F.; Boorn, A. W. Anal. Chem. 1984, 56, 875A-888A.
12. Ohls, K.; Sommer, D. Frezenius Z. Anal. Chem. 1979, 296, 241-246.
13. Jiang, S.-J.; Houk, R. S. Anal. Chem. 1986, 58, 1739-1743.
14. Human, H. C. G.; Scott, R. H.; Oakes, A. R.; West, C. D. Analyst 1976, 101, 265-271.
15. Scott, R. H. Spectrochim. Acta, Part B 1978, 33B, 123-125.

16. Marks, J. Y.; Formwalt, D. E.; Yungk, R. E. Spectrochim. Acta, Part B 1983, 38B, 107-113.

17. Thompson, M.; Goulter, J.; Sieper, F. Analyst 1981, 106, 32-39.

18. Carr, J. W.; Horlick, G. Spectrochim. Acta, Part B 1982, 37B, 1-15.

19. Gray, A. L. Analyst 1985, 110, 551-556.

20. Arrowsmith, P. Anal. Chem. 1987, 59, 1437-1444.

21. Drake, S. A.; Long, S. E.; Pickford, C. J.; Tyson, J. F. J. Anal Atom. Spectrom. 1989, 4, 715-719.

22. Arrowsmith, P. In Lasers and Mass Spectrometry; Lubman, D. E., Ed.; Oxford University Press: 1990; Chapter 8.

23. Pang, H.; Wiederin, D. R.; Houk, R. S.; Yeung, E. S., accepted for publication in Anal. Chem.

24. Sharp, B. L. J. Anal. Atom. Spectrom. 1988, 3, 613-652.

25. Sharp, B. L. J. Anal. Atom. Spectrom. 1988, 3, 939-963.

26. Broekaert, J. A. C.; Boumans, P. W. J. M. In Inductively Coupled Plasma Emission Spectroscopy--Part I; Boumans, P. W. J. M., Ed.; Wiley: New York, 1987; Chapter 6.

27. Meinhard, J. E. In Applications of Plasma Emission Spectrochemistry; Barnes, R. M., Ed.; Heyden: Philadelphia, 1979; pp. 1-14.

28. Hulmston, P. Analyst 1983, 108, 166-170.

29. Ramsey, M. H.; Thompson, M.; Coles, B. J. Anal. Chem. 1983, 55, 1626-1631.

30. Baginski, B. R.; Meinhard, J. E. Appl. Spectrosc. 1984, 38, 568-572.

31. Zhuang, H. Z.; Barnes, R. M. Spectrochim. Acta, Part B 1985, 40B, 11-19.

32. Scott, R. H.; Fassel, V. A.; Kniseley, R. N.; Nixon, D. E. Anal Chem. 1974, 46, 75-80.

33. Kniseley, R. N.; Amenson, H.; Butler, C. C.; Fassel, V. A. Appl. Spectrosc. 1974, 28, 285-286.

34. Novak, J. W.; Lillie, D. E.; Boorn, A. W.; Browner, R. F. Anal. Chem. 1980, 52, 576-579.

35. Anderson, H.; Kaiser, H.; Meddings, B. In Developments in Atomic Plasma Spectrochemical Analysis; Barnes, R. M., Ed.; Heyden: Philadelphia, 1981.

36. Boumans, P. W. J. M.; Lux-Steiner, M. Ch. Spectrochim. Acta, Part B 1982, 37B, 97-126.

37. Fujishiro, Y.; Kubota, M.; Ishida, R. Spectrochim. Acta, Part B 1984, 39B, 617-620.

38. Fry, R. C.; Denton, M. B. Anal. Chem. 1977, 49, 1413-1417.

39. Wolcott, J. F.; Sobel, C. B. Appl. Spectrosc. 1978, 32, 591-593.

40. Garbarino, J. R.; Taylor, H. E. Appl. Spectrosc. 1980, 34, 584-590.

41. Ripson, P. A. M.; de Galan, L. Spectrochim. Acta, Part B 1981, 36B, 71-76.

42. Layman, L. R.; Lichte, F. E. Anal. Chem. 1982, 54, 638-642.

43. Nisamaneepong, W.; Haas, D. L.; Caruso, J. A. Spectrochim. Acta, Part B 1985, 40B, 3-10.

44. Ibrahim, M.; Nisamaneepong, W.; Haas, D. L.; Caruso, J. A. Spectrochim. Acta, Part B 1985, 40B, 367-376.

45. Veillon, C.; Margoshes, M. Spectrochim. Acta, Part B 1968, 23B, 553-555.

46. Boumans, P. W. J. M.; DeBoer, F. J. Spectrochim. Acta, Part B 1976, 31B, 355-375.

47. Olson, K. W.; Haas, W. J., Jr.; Fassel, V. A. Anal. Chem. 1977, 49, 632-637.

48. Goulden, P. D.; Anthony, D. H. J. Anal. Chem. 1984, 56, 2327-2329.

49. Fassel, V. A.; Bear, B. R. Spectrochim. Acta, Part B 1986, 41B, 1089-1113.

50. Koropchak, J. A.; Winn, D. H. Anal. Chem. 1986, 58, 2558-2561.

51. Elgersma, J. W.; Maessen, F. J. M. J.; Niessen, W. M. A. Spectrochim. Acta, Part B 1986, 41B, 1217-1220.

52. Schwartz, S. A.; Meyer, G. A. Spectrochim. Acta, Part B 1986, 41B, 1287-1298.

53. Vermeiren, K.; Taylor, P. D. P.; Dams, R. J. Anal. Atom. Spectrom. 1987, 2, 383-387.

54. Koropchak, J. A.; Winn, D. H. Appl. Spectrosc. 1987, 41, 1311-1318.

55. Vermeiren, K. A.; Taylor, P. D. P.; Dams, R. J. Anal. Atom. Spectrom. 1988, 3, 571-577.

56. de Loos-Vollebregt, M. T. C.; Tiggelman, J. J.; Bank, P. C.; Degraeuwe, C. J. Anal. Atom. Spectrom. 1989, 4, 213-217.

57. Skogerboe, R. K.; Olson, K. W. Appl. Spectrosc. 1978, 32, 181-187.

58. Novak, J. W.; Browner, R. F. Anal. Chem. 1980, 52, 792-796.

59. Browner, R. F.; Boorn, A. W.; Smith, D. D. Anal. Chem. 1982, 54, 1411-1419.

60. Gustavsson, A. Spectrochim. Acta, Part B 1984, 39B, 85-94.

61. Canals, A.; Hernandis, V.; Browner, R. F. Spectrochim. Acta, Part B 1990, 45B, 591-601.

62. Xu, J.; Kawaguchi, H.; Mizuike, A. Anal. Chim. Acta 1983, 152, 133-139.

63. Vaughn, M. A.; Horlick, G. Appl. Spectrosc. 1986, 40, 434-445.

64. Tan, S. H.; Horlick, G. Appl. Spectrosc. 1986, 40, 445-460.

65. Hutton, R. C.; Eaton, A. N. J. Anal. Atom. Spectrom. 1987, 2, 595-598.

66. Gustavsson, A. Spectrochim. Acta, Part B 1988, 43B, 917-922.

67. Backstrom, K.; Gustavsson, A.; Hietala, P. Spectrochim. Acta, Part B 1989, 44B, 1041-1048.

68. Gustavsson, A.; Trends Anal. Chem. 1989, 8, 336-338.

69. McLaren, J. W.; Lam, J. W.; Gustavsson, A. Spectrochim. Acta, Part B 1990, 45B, 1091-1094.

70. Gustavsson, A.; Hietala, P. Spectrochim. Acta, Part B 1990, 45B, 1103-1108.

71. de Galan, L. Anal. Chem. 1986, 58, 697A-707A.

72. Thompson, J. J.; Houk, R. S. Anal. Chem. 1986, 58, 2541-2548.

73. Shabani, M. B.; Akagi, T.; Shimizu, H.; Masuda, A. Anal. Chem. 1990, 62, 2709-2714.

74. Nukiyama, S.; Tanasawa, Y. Trans. Soc. Mech. Eng., Tokyo 1938-1940, Vol. 4-6, Reports 1-6.

75. Plantz, M. R.; Fritz, J. S.; Smith, F. G.; Houk, R. S. Anal. Chem. 1989, 61, 149-153.

76. Viczián, M.; Lásztity, A.; Wang, X.; Barnes, R. M. J. Anal. Atom. Spectrom. 1990, 5, 125-133.

ACKNOWLEDGMENTS

It is difficult to adequately recognize those who have helped me throughout my graduate studies. First, I wish to acknowledge my wife, Michelle, for her love, patience, and for the sacrifices she has made over the last few years. I thank my son, Kevin, for the many happy times he has given me. I also want to acknowledge my parents, Ralph and Helen Wiederin, for all they have done for me, and for supporting me without question in endeavors which they did not completely understand. Thanks Mom and Dad. I thank Gene and Edna Doolan for the tremendous kindness and generosity they have shown me since I met their daughter, my wife.

I am also indebted to many people at Iowa State and Ames Laboratory for assisting me in countless ways. Above all I thank Sam Houk for his direction, suggestions, support, and tolerance. This thesis is a testament to Sam's indulgence in allowing me to pursue a variety of projects, many of which were not fruitful; to his uncritical support when experiments failed, to his helpful advice, and to his guidance in helping to communicate the research results to the scientific community.

I would also like to thank Art D'Silva for his insight, ideas, and friendship over the last four years. Of course, I owe the members of the Houk group deep appreciation not only for aid in experimental work, but for the friendship they have shown me during the time I have spent at Iowa State. I especially want to thank Fred Smith, Luis

Alves, H. Bin Lim, Sam Shum, Ke Hu, Shiuh-Jen Jiang, Bryant LaFreniere, and John Rowan. I also thank Jody Kolcker, Kevin Foje, and Ron Smyczek who helped with several projects as Ames Lab summer students. Finally, I thank Luis and Carla Alves for opening their home to me over the last months as I finished this thesis.

I would be remiss if I failed to acknowledge those who encouraged me to study chemistry before I entered graduate school. I thank my high school chemistry teacher Sister Francis Xavier for the extra time she spent helping me with projects after school and for teaching me that chemistry is fun. I also thank my undergraduate professors at Creighton University for providing excellent preparation for graduate studies. I especially thank Dr. Bruce Mattson, my undergraduate advisor, for his encouragement and for his efforts in helping me select a graduate program.

Several organizations have provided financial support. I gratefully acknowledge the National Science Foundation for the graduate fellowship which funded most of my studies. I also gratefully acknowledge Procter and Gamble for providing fellowship support this last year. I thank Cetac Technologies for providing an ultrasonic nebulizer. The Delavan Corporation generously provided the equipment for aerosol particle size measurements. I especially thank Sherm Conrad and Chuck Trullinger at Delavan for their help in arranging and conducting those experiments. Finally, Iowa State University and the Ames Laboratory provided additional financial support as well as excellent instrumental and technical facilities.